https://doi.org/10.5194/acp-2022-245
Preprint. Discussion started: 14 April 2022

Atmospheric Chemistry and Physics Discussions

Reconciling the total carbon budget for boreal forest wildfire emissions using airborne observations

Katherine L. Hayden[1]*, Shao-Meng Li[2], John Liggio[1], Michael J. Wheeler[1], Jeremy J.B. Wentzell[1], Amy Leithead[1], Peter Brickell[1], Richard L. Mittermeier[1], Zachary Oldham[1,6], Cris Mihele[1], Ralf M. Staebler[1], Samar G. Moussa[1], Andrea Darlington[1], Alexandra Steffen[1], Mengistu Wolde[3], Daniel Thompson[4], Jack Chen[1], Debora Griffin[1], Ellen Eckert[1], Jenna C. Ditto[5], Megan He[5] and Drew R. Gentner[5]

[1]{Air Quality Research Division, Environment Canada, Toronto, ON, Canada}
[2]{College of Environmental Sciences and Engineering, Peking University, Beijing, China}
[3]{National Research Council of Canada, Ottawa, ON, Canada}
[4]{Canadian Forest Service, Natural Resources Canada, Edmonton, AB, Canada}
[5]{Yale University, New Haven, CT, USA}
[6]{University of Waterloo, Waterloo, ON, Canada}

*Correspondence to: Katherine Hayden (katherine.hayden@ec.gc.ca)

Abstract

Wildfire impacts on air quality and climate are expected to be exacerbated by climate change with the most pronounced impacts in the boreal biome. Despite the large geographic coverage, there is a lack of information on boreal forest wildfire emissions, particularly for organic compounds, which are critical inputs for air quality model predictions of downwind impacts. In this study, airborne measurements of 250 compounds from 15 instruments, including 228 non-methane organics compounds (NMOG), were used to provide the most detailed characterization, to date, of boreal forest wildfire emissions. Highly speciated measurements showed a large diversity of chemical classes highlighting the complexity of emissions. Using measurements of the total NMOG carbon ($NMOG_T$), the ΣNMOG was found to be 46.2 % of $NMOG_T$, of which, the intermediate- and semi-volatile organic compounds (I/SVOCs) were estimated to account for 7.4 %. These estimates of I/SVOC emission factors expand the volatility range of NMOG typically reported. Despite extensive speciation, a substantial portion of $NMOG_T$ remained unidentified (46.4 %), with expected contributions from more highly-functionalized VOCs and I/SVOCs.

https://doi.org/10.5194/acp-2022-245
Preprint. Discussion started: 14 April 2022


Atmospheric Chemistry and Physics Discussions

The emission factors derived in this study improve wildfire chemical speciation profiles and are especially relevant for air quality modelling of boreal forest wildfires. These aircraft-derived emission estimates were further linked with those derived from satellite observations demonstrating their combined value in assessing variability in modelled emissions. These results contribute to the verification and improvement of models that are essential for reliable predictions of near-source and downwind pollution resulting from boreal forest wildfires.

https://doi.org/10.5194/acp-2022-245
Preprint. Discussion started: 14 April 2022


Atmospheric Chemistry and Physics Discussions

1 Introduction

Wildfires play a natural role in maintaining forest health and diversity through the release of nutrients, seed germination, removal of aging vegetation, and reducing the spread of forest diseases. Wildfires are, however, one of the largest global sources of trace gases and aerosols to the atmosphere (Andreae, 2019; Yu et al., 2019) and can have deleterious impacts on human health (Cascio, 2018; Cherry and Haynes, 2017; Reid et al., 2016; Finlay et al., 2012), air quality (Landis et al., 2018; Miller et al., 2011; Rogers et al., 2020), ecosystems (Kou-Giesbrecht et al., 2019; Campos et al., 2019; Kallenborn et al., 2012; Johnstone et al., 2010) and climate (Randerson et al., 2006). Not only can wildfire pollutants fumigate local source areas, they can be transported over long distances resulting in degraded air quality in locations far from fire sources (Miller et al., 2011; Rogers et al., 2020), and pose threats to downwind ecosystems through wet and dry deposition processes (Kou-Giesbrecht et al., 2019; Kallenborn et al., 2012; Campos et al., 2019).

Wildfire impacts on air quality and climate are expected to be exacerbated by climate change (Bush and Lemmen, 2019; Seidl et al., 2017; Whitman et al., 2019) and such impacts are expected to be most pronounced in the boreal biome (Seidl et al., 2017; Whitman et al., 2019). The boreal forest zone is the most northerly of all forest biomes accounting for 1.2 billion ha of mostly coniferous forest and comprising about 30 % of the global forest area, or 11 % of the earth's land surface. On a global basis, boreal forest wildfires are responsible for an estimated 20 % of yearly global biomass burning emissions (van der Werf et al., 2006). Canada's boreal forests account for ~30 % of the global boreal zone area and encompasses 75 % of Canada's 347 million ha of forested land (Fig. S1). In the past decade, Canada has experienced unprecedented fire seasons, with large numbers of evacuations, major property damage, poor air quality and significant economic impacts (NRCan, 2018; Landis et al., 2018; McGee et al., 2015). Model predictions have suggested that Canadian fire occurrences will increase by 25 % by 2030 from a 1975 to 1990 baseline scenario (Wotton et al., 2010).

To adequately assess and mitigate the risks of wildfire emissions to human and ecosystem health, reliable pollutant predictions are required which depend on accurate and detailed fire emissions data.

https://doi.org/10.5194/acp-2022-245
Preprint. Discussion started: 14 April 2022


Atmospheric Chemistry and Physics Discussions

Such emissions data are developed by multiplying emission factors and ratios with the mass of biomass burned (Chen et al., 2019). In Canada, Environment and Climate Change Canada (ECCC) provides predictions of particulate matter (PM) (<2.5 µm in diameter) from wildfire smoke to the public using the FireWork modelling system that combines forecast meteorology, emissions inputs (e.g. emission factors), forest fire and fuel data (e.g. fuel maps, plume height parameterization), and a regional air quality model, GEM-MACH (details in Chen et al., 2019). FireWork is also used for air quality research studies with significantly more complex chemical mechanisms for emissions characterization and detailed physical processes. Wildfire field studies, as well as prescribed burns and laboratory work, have resulted in valuable global databases of fire emission factors covering a broad range of ecosystems and geographic areas (e.g. Andreae, 2019; Akagi et al., 2011), however, they are primarily concentrated on the temperate forests of the American mid-west and savannah/grasslands of Africa (e.g. Andreae 2019; Permar et al., 2021; Palm et al., 2020; Lindaas et al., 2020; Roberts et al., 2020; Juncosa-Calaharrano et al., 2021; Coggon et al., 2019; Koss et al., 2018; Hatch et al., 2017). Due to a lack of emission data specific for boreal wildfires, air quality models for northern regions face significant challenges resulting in uncertain predictions of emissions, exposure and associated impacts.

In the summer 2018, a research aircraft was deployed to measure emissions and subsequent transformation processes from an active boreal forest wildfire in western Canada (Fig. 1; Fig. S1). In this paper, detailed emissions information is provided from an active, near-field boreal forest wildfire using a detailed measurement suite of over 200 gas- and particle-phase compounds. Emissions of highly speciated non-methane organic gases (NMOG) are characterized by broad chemical classes and volatilities extending from VOCs to SVOCs. Speciated NMOGs, along with concurrent total NMOG carbon ($NMOG_T$) measurements, provides a unique opportunity to reconcile the total carbon budget. Emission factors are derived for all measured compounds resulting in more relevant emissions information for boreal forest wildfires and improved emission quantification and chemical speciation representations in air quality models. Combining aircraft-derived emissions with those from satellite observations demonstrates usefulness to evaluate modelled emissions variability. The emissions

https://doi.org/10.5194/acp-2022-245
Preprint. Discussion started: 14 April 2022


Atmospheric Chemistry and Physics Discussions

information in this work will contribute to verification and improvements of models that are essential for reliable predictions of boreal forest wildfires pollutants.

2 Methods

2.1 Aircraft measurements

The NRC's Convair-580 research aircraft was deployed on June 25, 2018 to sample a wildfire detected to the east of the Alberta/Saskatchewan border (56.4°N, 109.7°W) (Fig. 1). Measurements of a comprehensive suite of trace gases, particles and meteorology were made with high time resolution. Meteorological measurements including relative humidity, temperature, wind direction and speed, as well as aircraft state parameters such as altitude (masl) and geographic coordinates were conducted at 1 sec intervals. A detailed description of the various measurements methods with references is provided in the supporting information (SI Sect. 2.1, Table S1), with only a brief description provided here.

2.1.1 Trace gas measurements In-situ measurements of NO, NO_2, NO_y, O_3 and SO_2 were conducted using commercial instruments (Thermo Scientific Inc.) modified to measure at 1 sec time resolution. Ammonia (NH_3) measurements were made at 1 sec time resolution using a Los Gatos Research (LGR) NH_3/H_2S Analyzer, model 911-0039. Calibrations were conducted periodically throughout the measurement study using NIST–certified standards. Instrument zeros were performed for all these instruments 3-5 times per flight for a duration of ~3-5 minutes each time at the beginning, during and after each flight. Gas phase elemental Hg (GEM) was measured with a Tekran 237X instrument (Tekran Instruments Corporation) modified to allow a reduced sampling time of 2 min (McLagan et al., 2021; Cole et al., 2014). CO, CO_2 and CH_4 were measured with a Cavity Ring Down spectroscopy instrument (Picarro G2401-m). A second Picarro G2401-m instrument was used to measure Total Carbon (TC, in units of ppmC) by passing the sample air through a platinum catalyst (Shimadzu) which was placed at the external rear-facing inlet assembly and maintained at 650 °C, adapted from Stockwell et al. (2018) and Veres et al., (2010). Total non-methane organic gases ($NMOG_T$), in mixing ratios units of ppmC, were

https://doi.org/10.5194/acp-2022-245
Preprint. Discussion started: 14 April 2022


Atmospheric Chemistry and Physics Discussions

quantified by subtracting the ambient CH_4, CO and CO_2 measurements (instrument without the upstream catalyst) from the TC measurements.

Individually speciated NMOGs (as well as some inorganic species) were measured with a Chemical Ionization Mass Spectrometer (CIMS), a Proton Transfer Time-of-Flight Mass Spectrometer (PTRMS), and through whole air sampling using canisters (Advanced Whole Air Sampler; AWAS). In addition, integrated cartridge-based samples were taken. The CIMS (a modified Tofwerk/Aerodyne Api-ToF) was operated using iodide as the reagent ion providing 1 sec time resolved measurements for 30 compounds (Table S2). The PTRMS (Ionicon Analytik GmbH, Austria) used chemical ionization with H_3O^+ as the primary reagent ion providing 1 sec measurements for a suite of organic compounds. For those compounds with no available gas standard, a relative response factor was calculated with reaction rate constants using the method described in Sekimoto et al. (2017) and guided by the work of Koss et al. (2018) ('calculated' compounds). Integrated 'grab' samples (20-30 sec) were collected from the aircraft using the Advanced Whole Air Sampler (AWAS) with offline analysis. The AWAS provided speciated measurements of hydrocarbons (<C10), but no oxygenates. Overlapping compounds/isomers that were measured by both the PTRMS and AWAS, as well as between the PTRMS and CIMS were handled as described in SI Sect. 2.1.4. Integrated gas phase samples were collected using an automated adsorbent tube (i.e. cartridge) sampling assembly with offline analysis (Ditto et al., 2021; Sheu et al., 2018; Khare et al., 2019). These samples provided targeted measurements of gas-phase compounds ranging in volatility from C_{10} volatile organic compounds (VOCs) to C_{25} semivolatile organic compounds (SVOCs) including hydrocarbons (CH), and functionalized compounds containing 1 oxygen atom (CHO_1), and 1 sulfur atom (CHS_1).

2.1.2 Particle measurements

Particle chemistry was obtained with a high resolution aerosol mass spectrometer (AMS) (Aerodyne) providing mass concentrations of particle species including total organics (OA), NO_3, SO_4 and NH_4 for particles less than ~1 µm. Particle size distributions were measured between 60 and 1000 nm at 1 sec time resolution using the Ultra High Sensitivity Aerosol Spectrometer (UHSAS; Droplet

https://doi.org/10.5194/acp-2022-245
Preprint. Discussion started: 14 April 2022


Atmospheric Chemistry and Physics Discussions

Measurement Technologies). Refractory black carbon (rBC) was measured using a single particle soot photometer (SP2; Droplet Measurement Technologies).

2.2 Flight and fire description

A wildfire located near Lac La Loche in Saskatchewan (56.40°N 109.90°W) was detected by satellite on June 23 (Fig. 1; Fig. S1). The fire was ignited by lightning on June 23, 2018 at 19:45 UTC and lasted 50 hrs to June 25 21:41 UTC burning an estimated 10,000 ha before being extinguished by rain. The area burned was mostly mature Jack pine and boreal spruce forest with a smaller fraction of boreal mixed-wood forest. Satellite images from the VIIRS spectroradiometer on the Suomi NPP and NOAA-20 satellites taken on June 25 showed merged fire hot spots with a visible smoke plume moving in a north-westerly direction (Fig. 1; see SI Sect. 2.2 for more details).

Lagrangian flight tracks were flown downwind of the wildfire to follow the fire plumes. Multiple horizontal transects, vertically stacked and perpendicular to the plume direction were made at different altitudes from 640 to 1460 m asl (~220 – 1040 m agl, based on 420 m asl at Lac La Loche) forming virtual screens. Five screens were completed over two flights with the closest screen ~10 km and the farthest screen 164 km downwind of the fire, with the screens spaced such that the instruments sampled the same air parcels as they were transported downwind. A vertical profile which typically reached ~2500 m asl was conducted in the plume at each screen to gather information on its vertical structure and the height of the plume. As demonstrated by the elevated CO mixing ratios in Fig. 2, two distinct plumes were identified - a south plume (SP) and north plume (NP), that were transported in parallel in a northwesterly direction. The SP is estimated to be ~42 min old based on the measured wind speed at Screen 1 and the distance from the closest edge of the VIIRS fire hot spots (~10 km). The NP is estimated to be an additional 30 min older than the SP (further details in SI Sect. 2.2). For the purposes of this investigation, only data from Screen 1 are used to characterize the direct emissions from this fire. Evaluation of emissions of photolabile species could be influenced by photochemical and depositinal losses that may take place between the time of emission and the time of measurement. However, at 10

https://doi.org/10.5194/acp-2022-245
Preprint. Discussion started: 14 April 2022


Atmospheric Chemistry and Physics Discussions

km (<1 hr) away from the fire source, Screen 1 measurements represent some of the freshest emissions ever measured under wildfire conditions. There are no other significant anthropogenic sources impacting the Screen 1 measurements. Plume evolution during transport from Screen 1 to downwind Screens 2 to 5 is discussed in other papers (Liu et al., 2022; Ditto et al., 2021; McLagan et al., 2021).

2.3 Emission ratios, emission factors and combustion efficiency

Emission ratios Emission ratios were calculated using an integration method (e.g. Yokelson et al., 2009) with the in-plume measurements for the SP and NP. The integration method was carried out by first subtracting a background from the in-plume measurements. Background measurements were defined as the average over short time segments (~30 sec) outside and at the same altitude as inside the plume, and typically selected at the ends of the horizontal transects. The background-subtracted plume measurements yielded enhanced plume values (e.g. $\Delta X(t)$) which were then integrated using the plume start and end times guided by when CO mixing ratios were above the CO background. Nominal plume time periods are indicated by the vertical grey bars in Fig. 3 which shows time series for CO, NMOG, OA and acetonitrile for the first 4 of 5 transects on Screen 1. Integrated pollutant values were subsequently normalized by the integrated values of CO (Eq. 1) to account for changes due to dilution producing emission ratios (ER) for the SP and NP for each transect on Screen 1.

$$ER = \frac{\int_{start}^{end} \Delta X(t)\,(dt)}{\int_{start}^{end} \Delta CO(t)(dt)} \quad (1)$$

CO is known to be a suitable dilution tracer as it has a long atmospheric lifetime of 1-4 months (Seinfeld and Pandis, 1998), is unreactive on the time scale of the measurements, and is a particularly good tracer for smoldering fires (e.g. Simpson et al., 2011). In this study, ERs were calculated using CO as it was well above background for the plumes measured, there were no other significant CO sources in the study area, and co-varied well with the majority of measurements.

https://doi.org/10.5194/acp-2022-245
Preprint. Discussion started: 14 April 2022

Atmospheric Chemistry and Physics Discussions

196 **Emission factors** Emission factors (EFs) were determined as the mass of species X emitted per unit mass
197 of dry fuel burned in g kg^{-1} assuming that all of the carbon in the fuel was released into the atmosphere
198 and measured (Ward and Radke, 1993; Yokelson et al., 2007), and that the mass fraction of carbon in the
199 fuel is constant. EFs were determined using Eq. 2 where F_c is the mass fraction of carbon in the fuel and
200 estimated to be 0.5 (de Groot et al., 2009 and references therein), mm_x is the molar mass of the compound
201 of interest, and mm_c is the molar mass of carbon, 12 g mol^{-1}, ΔX is the background-subtracted mixing
202 ratio or concentration of the species of interest, ΔTC is the background-subtracted total carbon. Total
203 Carbon (TC) (see Sect. 2.1) was directly measured and includes all the carbon mass in CO_2, CO, CH_4, and
204 $NMOG_T$, as well as that from particulate black carbon (rBC) and particulate organic carbon (OC) (which
205 were added to the TC), for a complete accounting of all the emitted carbon. For species measured in mass
206 concentration units, Eq. 2 was modified by converting TC to mass concentrations using the measured
207 temperature and pressure, and removing the molar mass ratio term.
208
209 $$EF\ \left(\frac{g}{kg\ f}\right) = F_c\ x\ 1000\ \left(\frac{g}{kg}\right) x\ \frac{mm_X}{mm_C}\ x\ \frac{\Delta X}{\Delta TC} \quad (2)$$
210
211 EFs were determined for the SP and NP for each transect averaged to obtain screen-averaged EFs for the
212 SP and the NP, as well as for both plumes together. There is a potential for inherent uncertainties with
213 this approach for calculating EFs and ERs as the ratios derived this way represent the average plume
214 composition and ignore the spatial heterogeneity in wildfire plumes (Liu et al., 2022; Decker et al., 2021;
215 Peng et al., 2020; Garofalo et al., 2019), chemical transformation processes, and can also be affected by
216 changing background levels.
217
218 **Combustion efficiency** Combustion efficiency (CE) is a useful indicator of the relative proportion of
219 flaming vs smoldering stages of combustion which has a significant influence on the chemical
220 composition of the smoke (see SI Sect. 3.1 for further details). Flaming fires have CE >0.90 (Yokelson et

https://doi.org/10.5194/acp-2022-245
Preprint. Discussion started: 14 April 2022


Atmospheric Chemistry and Physics Discussions

al., 1996) and smoldering fires are typically ~0.8 with a range of 0.65 to 0.85 reported in the literature (Akagi et al., 2011; Yokelson et al., 2003). A modified combustion efficiency (MCE) is commonly calculated assuming that CO_2+CO adequately represents all of the fuel carbon that has been volatilized and detected in ambient air. Here, as the TC in the plume was directly measured, ΔTC was used in Eq. 3 to improve on the estimation of the CE by accounting for all the sources of carbon. ΔCO_2 and ΔTC in Eq. 3 are the integrated, background-subtracted mixing ratios.

$$CE = \frac{\Delta CO_2}{\Delta TC} \quad (3)$$

3 Results and Discussion

3.1 Fire combustion state

The plume-averaged CE for the SP (transects 1 to 4) was 0.84±0.04 and for the NP (transects 1 to 3) 0.82±0.01. Transect 4 was excluded from the calculations for the NP because only a portion of the plume was detectable at this altitude (Fig. 3). The derived CE indicates that the fire was predominantly in a smoldering phase which is consistent with the satellite-derived fire intensities during the flight (see Fig. 10) and ground-based meteorological observations, and may reflect some residual smoldering combustion (RSC). It is estimated that emissions from this fire were sampled 14 hrs post flaming. Other chemical measurements from this flight also support that the fire was largely smoldering including the detection of elevated $C_2H_4O_2^+$ (levoglucosan fragment from the AMS), low NO_x levels (Lapina et al., 2008) (Fig. S2), and no detectable K^+ (from the AMS) (Lee et al., 2010). Significant spatial variability in the concentrations of many of the measured species were observed closest to the fire source, while the plumes became more well-mixed as they were transported downwind (Fig. S3). This highlights the complexities of assessing wildfire combustion processes (Ward and Radke, 1993), and in particular, boreal forests have been observed to exhibit greater variability in combustion efficiencies than for other vegetation types (Urbanski et al., 2009).

https://doi.org/10.5194/acp-2022-245
Preprint. Discussion started: 14 April 2022


Atmospheric Chemistry and Physics Discussions

3.2 General plume features

Most pollutants were strongly concentrated in the fire plumes with the exception of several sulphur-containing compounds and a few other VOCs (Table S6). In Fig. 3, the in-plume portions are highlighted by the grey vertical bars and the SP and NP are indicated as the aircraft flew at increasing altitudes to complete five horizontal transects. The lowest 4 transects showed enhanced pollutant levels while the 5th transect (not shown) was predominantly above the height of the plumes. Higher concentrations were generally observed in the SP compared to the NP, possibly because of some plume dilution in the NP resulting from a change in wind direction prior to sampling. The SP and NP were distinctly separated from each other, with pollutants typically dropping to background levels between the plumes. $NMOG_T$ mixing ratios varied between 100 ppbv to near 10 ppmv in-plume. CO and acetonitrile, often used as tracers of biomass burning (e.g. Wiggins et al., 2021; Landis et al., 2018; Simpson et al., 2011; de Gouw et al., 2006), reached 6.6 ppmv and 20 ppbv, respectively in the SP, while maximum OA concentrations reached 276 µg m^{-3}, above a background level of ~9.5 µg m^{-3}. OA was the largest contributor to particulate mass (PM) comprising over 90 % of the measured submicron mass with remaining portion comprised of BC, NO_3, NH_4, and SO_4 (Fig. S4). Integrated filter samples taken from the aircraft across Screen 1 also showed the presence of a diverse set of functionalized particle-phase organic compounds (Ditto et al., 2021).

The most abundant reactive nitrogen compounds (N_r) were in the forms of reduced nitrogen (85 %) with NH_3 comprising 41.7 % of ΣN_r (Fig. 4) and substantially lower nitrogen oxides i.e. NO_x < 1 ppbv. A large portion of unmeasured nitrogen-containing compounds found in these plumes was likely dominated by peroxyacetyl nitrate (PAN) (Liu et al., 2022). These observations are consistent with emissions from smoldering fires (Burling et al., 2011; Goode et al., 2000; McMeeking et al., 2009; Yokelson et al., 1996). Dominant proportions of reduced nitrogen in biomass burning emissions were also reported previously (Lindaas et al., 2020; Burling et al., 2011; Yokelson et al., 1996). Alkyl nitrates have been identified in biomass burning emissions, but their contributions to total N_r appeared to be small (Juncosa-Calahorrano

https://doi.org/10.5194/acp-2022-245
Preprint. Discussion started: 14 April 2022


Atmospheric Chemistry and Physics Discussions

et al., 2021; Roberts et al., 2020; Lindaas et al., 2020; Simpson et al., 2011; Alvarado et al., 2010; Singh et al., 2010).

3.3 Total carbon budget

3.3.1 NMOG chemical classes – PTRMS, CIMS, AWAS

In-plume mixing ratios and the relative contribution of individually measured NMOG species to the sum of those species (ΣNMOG) are shown for 13 chemical classes in Fig. 5. (See Fig. S5 for separate SP and NP chemical classes). The largest chemical classes include carbonyls (acids, aldehydes and ketones), alcohols, hydrocarbons (alkanes, alkenes, alkynes), aromatics (including furans, phenol, benzene and toluene), and nitriles. Hydrocarbons (i.e. C_xH_y) are responsible for just over half of the ΣNMOG (52.8 %) (Fig. S6), with 27.2 % identified as alkenes such as ethene, propadiene, and propene, 19.3 % alkanes, predominantly ethane, and 3.1 % alkynes, almost entirely acetylene. Non-aromatic oxygenates account for an additional 36.2 % of the ΣNMOG with roughly equal contributions (10.1 to 11.0 %) from acids, aldehydes and alcohols, and a smaller fraction from ketones (4.8 %). Including other oxygenated compounds such as furanoids and phenol/phenol derivatives, all oxygenates ($C_xH_yO_z$) comprise 41.4 % (Fig. S6), of the ΣNMOG.

A similar range of compound classes has been observed in previous field and laboratory studies, noting that the measured compound suite between studies varies to some extent. For example, some hydrocarbons, like 1-butene, ethane, propane, and isobutene measured in the present study were not included in Koss et al., (2018) results. Other studies have also found oxygenates to be a large portion of NMOG emissions across multiple fuel types, including those similar to the current study, ranging from 51 – 68 % (Permar et al., 2021; Koss et al., 2018; Gilman et al., 2015; Akagi et al., 2011) with a range of 25 – 55 % reported in Hatch et al. (2017). Comparisons between studies are influenced by differences in study measurement suites and variations in fuel composition. The fraction of NMOG oxygenates in the present study (41.4 %) was closer to those reported in Hatch et al. (2017) when only the most relevant fuel types of pine and spruce were considered (55 % and 43 %, respectively). Similar to previous work

https://doi.org/10.5194/acp-2022-245
Preprint. Discussion started: 14 April 2022


Atmospheric Chemistry and Physics Discussions

297 (Koss et al., 2018, Stockwell et al., 2015; Hatch et al., 2015), emissions of substituted oxygenates like
298 furanoids (furans+derivatives) and phenolic compounds were observed. Furanoids contributed 4 % of the
299 ΣNMOG mostly due to furfural, furan and methyl furan while phenolic compounds eg. guaiacol, methyl
300 guaiacol, contributed 0.5 % of the ΣNMOG (Fig. S7). Although their emissions were less abundant in the
301 present study, they represent important OH reactants (Coggon et al., 2019; Koss et al., 2018; Gilman et
302 al., 2015) with phenols being implicated as precursors to brown carbon formation in secondary organic
303 aerosol (SOA) (Palm et al., 2020).
304 Biogenic emissions of terpenoids including isoprene, monoterpenes, carvone, sesquiterpenes,
305 camphor/isomers and terpine-4-ol/cineole/isomers were elevated in the plumes collectively reaching 2.4
306 ppbv, and contributing ~1 % to the ΣNMOGs (Fig. S7). Isoprene was ~70 % of these compounds with an
307 additional 29 % from monoterpenes. Emissions of isoprene from biomass burning has been observed
308 from a wide range of fuel types (Hatch et al., 2019). As isoprene is not stored by plants and the
309 measurements were taken ~14 hrs post flaming, it was likely emitted as a combustion product.
310 In this study, furfural was the most abundant oxygenated aromatic compound, whereas Hatch et
311 al. (2015) and Koss et al. (2018) found that phenol emissions were slightly larger than that of furfural for
312 all fuels tested. As phenol emissions are associated with lignin pyrolysis (Stockwell et al., 2015;
313 Simoneit et al., 1999), the lower emissions in the current study could be because the lignin content in the
314 fuel mixture was lower than fuels used in previous studies or that most of the phenolic compounds were
315 emitted during the earlier phases of the fire. Several modelling studies have indicated that aromatics and
316 terpenes are insufficient to explain SOA formation in biomass burning plumes (e.g. Hodshire et al., 2019)
317 suggesting the importance of inclusion of other aromatic species such as phenolics and furanoid
318 compounds. However, models typically do not include reactions involving phenolic and furanoids
319 species, especially substituted compounds like furfural, guaiacol, and methyl guaiacol. Box model
320 simulations have also shown that incorporation of OH oxidation of furan, 2-methyfuran, 2,5-
321 dimethylfuran, furfural, 5-methylfurfural, and guaiacol, leads to 10 % more O_3 formed (Coggon et al.,
322 2019).

https://doi.org/10.5194/acp-2022-245
Preprint. Discussion started: 14 April 2022


Atmospheric Chemistry and Physics Discussions

3.3.2 Intermediate-volatility and semivolatile organic compounds (I/SVOCs)

Offline analysis of cartridge samples showed a wider range of hydrocarbons and functionalized gas-phase organic compounds not observed in the PTRMS, CIMS, and AWAS measurements, including I/SVOC compounds in the wildfire plume. ERs (Table S7) for species containing carbon, sulfur and oxygen (i.e. CH (hydrocarbons), CHS_1 and CHO_1 type molecules) accounted for a sizeable fraction of carbon in this range, with expected contributions from more highly functionalized organics in the gas (and particle) phase not reflected in the CH, CHO_1, and CHS_1 compound classes (e.g., gas-phase species with multiple oxygen atoms like vanillic acid or acetovanillone, and gas-phase species containing combinations of oxygen and nitrogen atoms (CHON) (Ditto et al., 2021; 2022). ERs in the plume varied across the carbon number range; in general, the highest ratios were observed for the complex mixture of hydrocarbons (i.e. CH compounds) broadly peaking at C_{20}-C_{25} in the SVOC range, with a larger contribution from C_{10} compounds including monoterpenes. By comparison, the complex mixture of CHO_1 compounds was slightly lower in abundance than CH with contributions from C_{10} monoterpenoid emissions or oxidation products. CHS_1 IVOC-SVOCs were the lowest abundance species quantified. CHN_1 compounds represent another observed contributor of IVOCs-SVOCs; the sum of all CHN_1 compound ion abundances was two orders of magnitude smaller than the sum of all CHO_1 species. We note that for CHN_1, this qualitative comparison is in terms of ion abundances only, given a lack of appropriate standards to calibrate for the complex mixture of reduced nitrogen I/SVOCs.

EFs were estimated for CH, CHO_1, and CHS_1 I/SVOCs based on Table S7 ERs (to CO) and the average EF of CO (115.7 ± 7.5 g kg^{-1}, Table A1). It was not possible to directly calculate EFs due to the lack of a background sample upwind of the fire. EFs were estimated to be 1.6±0.04 g kg^{-1} for CH, 0.9±0.09 g kg^{-1} for CHO_1, and 0.1±0.003 g kg^{-1} for CHS_1 species, for a total EF of 2.6±0.14 g kg^{-1} (Table A1). These estimates accounted for C_{11}-C_{25} species and focused on I/SVOCs to avoid double counting the monoterpenes and C_{10} monoterpenoid species. It is noted that the concentrations estimated for the cartridge samples may be sensitive to variations in sampling efficiency within the under-wing sampling pod across C_{10}-C_{25} (Ditto et al., 2021). These emission estimates expanded the characterized spectrum of

https://doi.org/10.5194/acp-2022-245
Preprint. Discussion started: 14 April 2022


Atmospheric Chemistry and Physics Discussions

organic species to include IVOC/SVOCs in boreal forest fire emissions, which until now, had only been available from laboratory measurements (Hatch et al., 2018). However, the observed emissions of the complex mixture of hydrocarbons and functionalized species may include contributions from the re-volatilization of compounds previously emitted from upwind oil sands operations and deposited in the forest ecosystem, as noted in Ditto et al. (2021).

3.3.3 Accounting for the observed carbon

Measurements of TC, along with the speciated measurements from the PTRMS, CIMS, AWAS and cartridges, provided a unique opportunity to reconcile the TC budget in a wildfire. Fig. 6 shows the TC partitioning based on derived EFs (Sect. 3.5); overlapping compounds from the individual measurement methods were handled as described in SI Sect. 2.1.4. The total EF for all carbon-containing compounds was 1651.5 g C kg^{-1} and, as expected, CO_2 was the dominant contributor comprising >90 % of TC. CO contributed 7.0 % followed by a contribution from $NMOG_T$ of 1.9 % with even smaller contributions observed from CH_4 (0.5 %) followed by OC and BC (not shown) at <0.5 %. The magnified pie chart (right side) displays the ΣNMOG EFs (for PTRMS+CIMS+AWAS measurements) totalling 14.4±3.2 g C kg^{-1} which accounted for 46.2 % of the $NMOG_T$ EF of 31.2±3.8 g C kg^{-1} (refer to Fig. S8 for the individual SP and NP breakdowns). The cartridge data showed the presence of a range of larger molecular weight I/SVOC compounds between C_{10} and C_{25} representing an additional 2.3±0.08 g C kg^{-1} and 7.4 % of $NMOG_T$. Together, all of the speciated NMOG measurements in this study accounted for 53.6 % of $NMOG_T$. The remaining carbon mass was unidentified comprising 46.4 % of $NMOG_T$. Despite using four state-of-the-art measurement techniques resulting in an extensive measurement suite, almost half of $NMOG_T$ remained unidentified. This is consistent with previous work estimating ~50 % of $NMOG_T$ by mass as unidentified (Akagi et al., 2011). It is noted, however, that the magnitude of the unidentified portion is partly affected by uncertainties in the speciated measurements. For example, many of the 'calculated' PTRMS compounds are uncertain by a factor of ~2 (SI Sect. 2.1.1, Table S1). Nevertheless, a portion of the unidentified species likely consisted of challenging-to-measure-VOCs and

https://doi.org/10.5194/acp-2022-245
Preprint. Discussion started: 14 April 2022


Atmospheric Chemistry and Physics Discussions

larger I/SVOCs that were highly functionalized or contained molecular features like reduced nitrogen groups (e.g. amines) that have been observed in the gas and particle phase at various sites (Ditto et al., 2020; Ditto et al., 2022). While a complex mixture of I/SVOCs were observed from this fire (Table S7), it is likely that other functionalized gas-phase species containing nitrogen and/or multiple oxygens (e.g. $CHO_{>1}$, CHON, CHN) were also emitted, similar to particle-phase observations in the fire plume via tandem MS in Ditto et al. (2021). The presence of I/SVOCs in biomass burning emissions has been previously observed in laboratory experiments (e.g. Koss et al., 2018; Hatch et al., 2018; Hatch et al., 2017; Bruns et al., 2016) with smoldering more likely to emit a higher fraction of compounds with low volatility than higher temperature processes (Koss et al., 2018). Advancing analytical techniques to expand the suite of NMOG speciation will enable further reconciliation of the TC budget which is important for assessing secondary formation processes in the atmosphere.

3.3.4 Volatility distribution of NMOG

Volatility distributions can help track the full range of organic species to assess their partitioning between the condensed and gas phases (Donahue et al., 2011). Fig. 7 shows the fractional sum of all NMOG EFs within each volatility bin in terms of saturation concentration ranges ($\log_{10}C_o$, μg m^{-3}). C_o values were estimated using the parameterization developed by Li et al. (2016). NMOG emissions from this fire spanned a large range of volatilities from $\log_{10}C_o$ of -2 to 10 μg m^{-3} across SVOCs to VOCs categories. The bin-averaged O/C ratio based on the measurements increased with reduced volatility reflecting the presence of compounds with additional oxygen-containing functional groups. The highest fraction of emissions was present as VOCs with 63.3 % having $\log_{10}C_o > 6$ μg m^{-3}, and 11.6 % as IVOCs having $4 < \log_{10}C_o$ μg $m^{-3} < 6$ μg m^{-3} and 7.9 % as SVOCs having $\log_{10}C_o < 3$ μg m^{-3}. These results align with laboratory studies showing that oxygenates comprised more than > 75 % of IVOCs across a range of biomass types with IVOCs accounting for ~11 % of the ΣNMOG (Hatch et al.; 2018). Fig. 7 encompasses the range of volatilities based on all the identified NMOGs in this study that is expected to represent initial emission conditions for modelling downwind chemistry. However, improved speciation,

https://doi.org/10.5194/acp-2022-245
Preprint. Discussion started: 14 April 2022


Atmospheric Chemistry and Physics Discussions

401 particularly of lower volatility compounds, are needed to further expand the range of volatilities and
402 advance knowledge in gas to particle partitioning processes.
403
404 **3.4 Emission factors and comparisons with other studies**
405 Emission factors (EF) (and emission ratios (ER)) in this study are derived for 250 compounds
406 from 15 instruments of which 228 are NMOG species (Table A1). This dataset represents the most
407 extensive range of field-based EFs ever determined for a wildfire in the boreal forest ecosystem. In Fig. 8
408 average EFs are shown for compounds grouped by a) particles, b) gas-phase inorganics, and c) gas-phase
409 organics. Separate EFs and ERs for the SP and NP are shown in the SI (Figs. S9 to S11). In Fig. 9a-c,
410 EFs are compared with those from other relevant studies. Fig. 9a shows a comparison with boreal forest
411 field measurements largely taken from a compilation by Andreae (2019) referred to as BFF19, as well as
412 values from Akagi et al. (2011) and Liu et al. (2017). This results in a comparison for 50 compounds (35
413 organics and 15 inorganics/particulate species) with the largest suite of EFs from one study conducted in a
414 similar boreal region as the present study (Simpson et al., 2011). EFs are also compared with laboratory-
415 derived EFs for lodgepole pine Koss et al. (2018; referred to as LAB18) (Fig. 9b), a dominant fuel in the
416 current study, with a total of 99 NMOGs and 3 inorganics in common. In Fig. 9c, EFs are compared with
417 those recently reported in Permar et al. (2021) (referred to as TFF21) based on aircraft measurements of
418 temperate forest wildfires which provides the closest suitable comparison with similar speciated NMOGs
419 under wildfire conditions. Comparisons include 111 NMOGs, and 4 inorganics/black carbon. While the
420 Permar et al. (2021) study was conducted in a temperate forest region, it was at high elevation locations
421 with similar vegetation types as the current study.
422
423 **3.4.1 Particle species** The PM_1 EF (6.8±1.1 g kg^{-1}) represents the total of all particle component species
424 as measured by the AMS. OA has the largest EF, accounting for 90 % of PM_1, with comparatively lower
425 EFs for pNO_3, rBC, pNH_4, and pSO_4 (Fig. 8a, Fig. S4). This reflects the dominant particle-phase organic
426 carbon content of the burned fuel and correspondingly lower fractions of nitrogen and sulphur-containing

https://doi.org/10.5194/acp-2022-245
Preprint. Discussion started: 14 April 2022


Atmospheric Chemistry and Physics Discussions

compounds. Similar high organic fractions have been previously observed in biomass burning emissions (Liu et al., 2017; May et al., 2014; Hecobian et al., 2011). ERs similarly highlight the dominant OA emissions. The magnitude of EFs and ERs are generally similar between the SP and NP. EFs and ERs for particle species derived in this study represent the first such measurements under boreal forest wildfire conditions. In Fig. 9a, EFs for chemically speciated compounds are not found in BFF19, but when compared with available values for U.S. temperate forest wildfires (Liu et al., 2017) are found to be lower for OA, SO_4, NO_3 and NH_4 by factors of 2.7, 5, 5.3, and 3.1, respectively. The lower particulate emissions in the present study may reflect differences in fuel elemental composition between temperate and boreal forest ecosystems. Differences in fuel composition is inferred through comparisons of NO_x and SO_2 emissions. For example, the average NO_x and SO_2 EFs for boreal forests, are lower than the average EFs for temperate forests by factors of 2.5 and 3.0, respectively. The lower NO_x and SO_2 emissions from boreal vs temperate forest wildfires are likely reflective of the reduced S and N content in boreal biomass (Bond-Lamberty et al., 2006) relative to conifer (Misel, 2012) fuels in the western U.S., as well as the possible influence of lower anthropogenic sources of nitrogen and sulphur atmospheric deposition in boreal forests (Jia et al., 2016). The PM_1 EF of 6.85±1.09 g kg^{-1} derived in the present study is a factor of 2.8 lower than the $PM_{2.5}$ EF of 18.76±15.90 g kg^{-1} that is available for BFF19 (Fig. 9b). The lower PM emissions in the present study, despite accounting for particle diameter differences (Sect. 2.1.2), is somewhat surprising given emissions of PM are typically higher from smoldering compared to flaming fires (Liu et al., 2017; Akagi et al., 2012). However, there are few PM EFs for BFF19 (n=5) over a limited range of MCEs (i.e. 0.89 to 0.93) showing significant variability. The PM_1 EF derived in the present study falls within the range previously observed for boreal forest wildfires and underscores the significant variability in PM emissions.

3.4.2 Gas-phase inorganic species The largest average EFs for inorganic gases (Fig. 8b) were from reduced nitrogen compounds dominated by NH_3 (0.63±0.19 g kg^{-1}) and followed by HCN (0.31±0.028 g kg^{-1}), with lower EFs for oxidized nitrogen compounds such as NO_2 (0.11±0.037 g kg^{-1}) and HONO

https://doi.org/10.5194/acp-2022-245
Preprint. Discussion started: 14 April 2022


Atmospheric Chemistry and Physics Discussions

453 (0.01±0.008 g kg^{-1}). This is consistent with previous work identifying elevated emissions of NH_3 and
454 HCN during smoldering conditions, whereas emissions of HONO and NO_x are primarily associated with
455 flaming combustion (e.g. Roberts et al., 2020; Akagi et al., 2013; Yokelson et al., 1997; Griffith et al.,
456 1991). The EFs for CO_2 and CO from the present study are very close to that previously reported for
457 BFF19 (Table A1). However, EFs for most other gaseous inorganic species were lower than the BFF19
458 EF average including NH_3, HONO, SO_2 (n=2) and NO_x (n=11), by factors of 3.9, 41, 4.7 and 14.9,
459 respectively (Fig. 9a). There are only a limited number of studies reporting EFs for these compounds in
460 the BFF19 category. For example, the HONO EF can only be compared with one other BFF19 study, but
461 is also lower compared to LAB18 (Fig. 9b). There are also only 4 previously reported BFF19 EFs for
462 NH_3 (2.46±1.75 g kg^{-1}) showing a large range of values indicating a strong sensitivity towards factors like
463 fire intensity and chemical reactivity. In contrast, EFs for HCN derived in the current study (0.31±0.028
464 g kg^{-1}) compare fairly well with BFF19, LAB18 and TFF21, (Figs 9a, b, c, respectively) and do not vary
465 widely suggesting that HCN may be less sensitive to burning characteristics. HCN is of concern due to
466 its impacts on human health particularly since biomass burning emissions are responsible for the majority
467 of the global HCN (Moussa et al., 2016 and references therein).
468
469 **3.4.3 Gas-phase organic species** In Fig. 8c, the top 25 average EFs for gas-phase organic species are
470 shown in decreasing order of magnitude. The most abundant emissions were from the lower molecular
471 weight compounds; such trends are generally in agreement with previous field-based measurements for a
472 range of fuel types (e.g. Permar et al., 2021; Andreae, 2019; Liu et al., 2017; Simpson et al., 2011;
473 Urbanski et al., 2009). Excluding CH_4, the largest EFs were associated with methanol, followed by
474 ethene, ethane, acetic acid, C_5 oxo-carboxylic acids, acetaldehyde, formaldehyde, and acetone ranging
475 from 1.9±0.25 g kg^{-1} to 0.82±0.088 g kg^{-1} for these compounds. Noting some variations related to
476 differences in measurement methods, other studies have identified many of these same species as
477 dominating biomass burning emissions (e.g. Permar et al., 2021; Simpson et al., 2011; Akagi et al., 2011).
478 For example, Simpson et al. (2011) found that 5 of the same compounds in the present study including

https://doi.org/10.5194/acp-2022-245
Preprint. Discussion started: 14 April 2022


Atmospheric Chemistry and Physics Discussions

formaldehyde, methanol, ethene, ethane and acetone were in the top 10 NMOG EFs from aircraft-based measurements made of boreal forest wildfires in northern Saskatchewan, Canada, and within ~300 km of the current study. In the present study, the top 24 NMOG compounds accounted for just over half (57 %) of the ΣNMOG by total molecular mass with lower lower emissions from the remaining measured compounds. In western U.S. wildfires, small emissions from 151 species were found to account for almost half of ΣNMOG (Permar et al., 2021).

To compare the total NMOG derived in the present study with those from previous studies that typically sum up their speciated measurements i.e. ΣNMOG, estimates were made using two methods: 1. increasing the ΣNMOG to account for the unidentified portion of $NMOG_T$; and 2. adjusting the $NMOG_T$ to reflect the total molecular mass (not just the carbon portion). For method 1, the ΣNMOG EF in this study (25.8±3.2 g kg^{-1}) was increased by 46.4 % (Fig. 6) equalling 37.8 g kg^{-1}. This estimate assumes that the carbon distribution is the same as the identified, speciated measurements. For method 2, based on the speciated measurements, the average molecular mass was 100 g mol^{-1} and the average carbon number was 6 resulting in ~28 % of the molecular fraction represented by atoms other than carbon. Adjusting the $NMOG_T$ of 31.2±3.8 g C kg^{-1} upwards by 28 % to reflect the additional molecular mass results in a $NMOG_T$ of 39.9 g kg^{-1}. The resulting estimated $NMOG_T$ in this study of 37.8 to 39.9 g kg^{-1} lies between the estimated average of 58.7 g kg^{-1} for the BFF19 (Fig. 9a) and those estimated from the ΣNMOG EFs of 25.0 g kg^{-1} (LAB18) (Fig. 9b), and 26.1±6.9 g kg^{-1} (TFF21) (Fig. 9c) derived from laboratory- and field-based studies. In contrast to the current work, previous estimates of $NMOG_T$ are likely to underestimate total NMOG emissions as they typically represent the sum of measured species only. Some studies have attempted to account for $NMOG_T$ by including the sum of measured plus estimates of 'unknown' portions of NMOGs (ΣNMOGs) (Permar et al., 2021; Koss et al., 2018; Stockwell et al., 2015; Gilman et al., 2015). The BFF19 EF was recently doubled from 29.3±10.1 g kg^{-1} to 58.7 g kg^{-1} to account for unidentified NMOGs where the ΣNMOGs were measured by FTIR, GC and PTRMS (Andreae, 2019; Akagi et al., 2011). These results support that doubling the ΣNMOG provides a reasonable estimate the $NMOG_T$. It is noted, however, that the average BFF19 NMOG EF is ~1.5 times higher than that derived

https://doi.org/10.5194/acp-2022-245
Preprint. Discussion started: 14 April 2022


Atmospheric Chemistry and Physics Discussions

in the present study, however, this may reflect variability in NMOG emissions even within the same boreal biome.

Although it is known that acidic compounds are emitted from biomass burning, few studies have quantified their emission, particularly under field conditions (Andreae, 2019; Veres et al., 2010; Yokelson et al., 2009; Goode et al.; 2000). In this study, EFs for 31 organic acidic compounds were derived (Table A1) representing the most detailed set of organic acid EFs from biomass burning for any ecosystem (Andreae, 2019). The largest EFs for these compounds include acetic acid, C5 oxo-carboxylic acids, C4 oxo-carboxylic acids, and pyruvic acid, all of which are found among the top 24 NMOGs (Fig. 8c). For those measurements that are available for comparison, EFs in the present study were lower for formic acid and acetic acid, than in BFF19, and were also lower than in LAB18, and TFF21, ranging from factors of 1.7 to 8.8 (Figs. 9c, d). A total of nine organic acids that were in common with TFF21 and LAB18 (Table A1) have lower EFs, with the exception of pyruvic acid, which was substantially higher (> factor of 37) in the present study. Emissions for an additional 23 organic acids, as well as several inorganic acids including nitrous acid, isocyanic acid, and peroxynitric acid, are included in Table A1. These acids, representing 10.3 % of the ΣNMOGs (Fig. 5), are an important class of oxygenates as they can form additional PM (Reid et al., 2005) and influence the hygroscopicity of smoke particles (Rogers et al., 1991; Kotchenruther and Hobbs, 1998).

Isoprene and monoterpenes, with similar EFs ~0.40±0.10 g kg^{-1}, represented 17th and 20th, respectively, of the top 24 NMOG EFs in this study. Terpenes are known to be emitted from a range of biomass burning fuels (Andreae, 2019 and references therein), but there have been few measurements in boreal forest wildfire plumes (Simpson et al., 2011; Andreae, 2019). It is noted that PTRMS measurements of IVOCs like sesquiterpenes likely represent lower limits as they tend to be easily lost to sample inlet lines due to their low volatility. The isoprene EF of 0.41±0.10 g kg^{-1} was more than a factor of 5 higher, while the monoterpenes EF, 0.39±0.034 g kg^{-1}, was substantially lower than the only reported EF for boreal forest wildfires (Simpson et al., 2011). As the present study and the Simpson et al. (2011) study were conducted in similar locations (i.e. boreal forest region within ~300 km of each other), with

https://doi.org/10.5194/acp-2022-245
Preprint. Discussion started: 14 April 2022


Atmospheric Chemistry and Physics Discussions

similar average MCEs, and comparable background levels, these differences are likely driven by fire stage sampled. The majority of monoterpenes are stored in plant tissues (resin stores) for long periods of time, but isoprene is synthesized and immediately released by plants, and can also be emitted as a combustion product (Ciccioli et al., 2014; Akagi et al., 2013). Hatch et al. (2019) found that a wide range of terpenoids are released across a variety of biomass types with variable emissions that were dependent on plant species, and specifically related to their fuel resin stores. In the present study, monoterpenes may have 'boiled-off' through distillation processes in the early stages of the fire resulting in lower monoterpenes emissions at the aircraft sampling time, ~14 hrs post-flaming. In contrast, the Simpson et al. (2011) study sampled comparatively earlier and more intense fire stages where higher monoterpene emissions were likely released from live or recently fallen trees that still contained significant resin stores. The monoterpenes EF reported by Simpson et al. (2011) was likely even higher given only two monoterpenes were speciated and emissions of other terpenes were likely (Hatch et al., 2019). Higher isoprene emissions in the present study compared to Simpson et al. (2011) could be related to the comparatively larger smoldering component. Although limited data exist on the release of isoprene as a function of fire intensity, negative relationships between isoprene and MCE were observed in Australian temperate forest fires (Guérette et al., 2018) and wheat fields (Kumar et al., 2018).

Several furanoid compounds also exhibited significant emissions (Fig. 8c) including furfural, furan, and methyl furan ranking 12th, 19th, and 23rd of the top 24 NMOG compounds, respectively. Emissions of furanoids have been observed for a wide range of fuel types (Hatch et al., 2017; Simpson et al., 2011). Fairly good agreement was found with BFF19 for furfural, and furan (Fig 9a). The EFs for furan (0.39±0.028 g kg^{-1}) and furfural (0.65±0.08 g kg^{-1}) were also similar to that in LAB18 (Fig. 9b), and TFF21 (Fig. 9c), as well as other ecosystems (Andreae, 2019) suggesting their emissions were relatively insensitive to fire intensity and fuel mixture. Overall, the comparisons in Fig. 9 indicate that for the higher emitting species, the current results are fairly similar, but for the lower emitting species, these results are lower than previous reported values.

https://doi.org/10.5194/acp-2022-245
Preprint. Discussion started: 14 April 2022


Atmospheric Chemistry and Physics Discussions

3.5 Evaluation of emissions models

3.5.1 Comparison of EFs with the model emissions speciation profile

EFs derived in the present study are compared with those that are currently incorporated into the emissions component of the FireWork modelling system using the Forest Fire Emissions Prediction System (CFFEPS). CFFEPS uses EFs allocated for 3 combustion states (flaming, smoldering and residual) and for 8 species including lumped non-methane hydrocarbons (NMHC) based on United States vegetation data compiled in Urbanski et al. (2014) (Table 3 in Chen et al., 2019). Fig. 9d (bolded compounds) shows that the smoldering EFs in the present study were comparable for CO and CH_4, but lower for PM_1 ($PM_{2.5}$), NH_3, SO_2 and NO_x by factors of 3.4, 2.4, 6.6 and 17, respectively. In the present study, additional mass between PM_1 and PM_{25} accounted for only an additional 10 % of aerosol mass (SI Sect. 2.1.2). The lower EFs for these species implies that the CFFEPS EFs would not adequately capture their total emissions under smoldering conditions for the boreal fuel in the current measurement study.

For incorporation into numerical air quality models, total organic gas (TOG=NMOG+CH_4) emissions are typically split into detailed chemical components using chemical mass speciation profiles, and converted to lumped chemical mechanism species. In the FireWork modelling system, the smoldering combustion TOG is split into components based on EPA's SPECIATEv4.5 profile (#95428) (US EPA 2016, Urbanski et al.; 2014 - supplement Table A.2, Boreal Forest Duff/Organic soil). This profile is ultimately compiled using laboratory data from Yokelson et al. (2013), Bertschi et al. (2003), and Yokelson et al. (1997) based entirely on U.S fuel types. EFs in the present study were found to be generally lower than the laboratory-based EFs for 74 species in common ranging from factors of 1.7 to 8.5 including for monoterpenes, formic acid, phenol, furan and acetonitrile (Fig. 9d). The largest differences (factors of 49-57) were observed for sesquiterpenes, benzofuran, and naphthalene. A few species including furfural, propane nitrile and ethyl styrene are comparable, while isoprene, pyruvic acid, acetylene and cyclohexene are notably higher by factors 2 to 5.3.

For a research version of the FireWork system, the component speciation is mapped to the SAPRC-11 chemical mechanism species (Carter and Heo, 2013) with detailed oxygenated compounds

https://doi.org/10.5194/acp-2022-245
Preprint. Discussion started: 14 April 2022


Atmospheric Chemistry and Physics Discussions

and aromatic species, largely to better represent SOA formation processes. For comparison with the measurement derived speciation profile in this study, EFs were first mapped to SAPRC-11 species and then normalized to obtain mass fractions of relevant model mechanism species (Table S9). Comparing the normalized mass fractions for similar mechanism species (Fig. S12) showed much lower fractions of reactive alkenes (ALK5) and aromatics (ARO2) and a slightly higher acetic acid group (CCOOH). The mass fraction of CH_4 is also different with 13 % of TOG in this study compared to 4 % from the SAPRC-11 profile. The measurement derived chemical speciation profile is expected to be slightly different from the average speciation profile from EPA's SPECIATEv4.5 due to fuel type, chemical species identification and mechanism mapping scheme. The emissions profile developed in the present study is considered a more representative smoldering emissions profile specific to the wildfire characterization for the Canadian boreal forest fuel.

3.5.2 Linking aircraft and satellite observations to evaluate modelled emissions diurnal variability

Wildfires generally exhibit a diurnal cycle with fire intensities maximizing late afternoon and diminishing at night having important implications for fire emissions. Evaluating modelled emissions throughout the diurnal cycle with observations is a critical step in verifying smoke predictions. Emissions models mostly parameterize diurnal fire emissions with prescribed profiles that distribute daily total emissions to hourly. In CFFEPs, a diurnal profile is applied to allocate daily burn area to hourly intervals, with highest activity in the late afternoon. The actual fuel consumed, and thus, hourly emissions, is then calculated with depth of burn estimates driven by hourly meteorology (Chen et al., 2019). In Fig. 10, for the wildfire in the present study, the hourly CFFEPS-predicted emissions (orange dots) for selected compounds are shown between 2018-06-24 17:00 UTC and 2018-06-25 21:00 UTC, spanning the aircraft sample time (red arrow at 15:00 UTC). The burning phases are outlined in the figure where flaming (light pink background) is assumed to occur when the atmospheric conditions alongside fire behaviour and emissions model outputs infer a fireline intensity >4,000 kW m^{-1}, and a smoldering fire (blue background) for intensity <4000 kW m^{-1}. The fire intensity distinction between flaming and smoldering

https://doi.org/10.5194/acp-2022-245
Preprint. Discussion started: 14 April 2022


Atmospheric Chemistry and Physics Discussions

610 roughly aligns with the observed minimum for this particular fire with the fire radiative power (FRP, grey
611 dots) retrieval from the GOES-16 satellite sensor of 500 MW where smoldering occurs <500 MW and
612 flaming for >500 MW. The 500 MW threshold over the approximately 1,700 ha of actively smoldering
613 area observed by overnight VIIRS thermal detections gives an estimated energy density of 0.29 MW ha^{-1}.
614 This FRP per unit area corresponds with observed FRP for flaming combustion of >0.4 MW ha^{-1} from
615 lower intensity flaming fires by O'Brien et al. (2015). The FRP represents the sum over all hotspots of
616 this fire for each 15-min observation period. Emission rates in metric tonnes per hour (t h^{-1}) were derived
617 from selected aircraft measurements using a mass balance method (Gordon et al., 2015) and estimated to
618 be 29±2.1 t h^{-1} for PM_1, 433±26.7 t h^{-1} for CO, 0.65± 0.03 t h^{-1} for NO_x (as NO), and 2.7±0.16 t h^{-1} for
619 NH_3 (red arrows). Emission rates were also derived from satellite observations (black arrows) for CO,
620 NO_x, and NH_3. Emissions of CO were estimated using a flux method as described in Stockwell et al.
621 (2021) using TROPOMI satellite observations yielding 1670±670 t h^{-1} at 19:06 UTC and 4050±1620 t h^{-1}
622 at 20:48 UTC. NO_x emissions (9.1±3.4; scaled to t NO h^{-1} at 19:06 UTC (not enough high-quality
623 observations for the 20:48 UTC overpass) were derived from the TROPOMI NO_2 dataset using an
624 Exponentially Modified Gaussian approach (Griffin et al., 2021). NH_3 emission rates (5.6±3.9 t h^{-1}) were
625 derived from CRIS satellite observations at the satellite overpass time of 19:00 UTC by applying a flux
626 method (Adams et al., 2019).

627 The aircraft measurements were taken when the FRP was low reflecting a smoldering surface
628 fire. However, the satellite overpass occurred ~4 hrs later than the aircraft measurements close to the
629 FRP daily maximum, after which rain passed through the area. The CFFEPS model, exhibiting a
630 prescribed diurnal pattern, captures the increase in NO_x and NH_3 emissions between that derived from the
631 aircraft and satellites transitioning from a smoldering to predominantly flaming fire; NO_x emissions
632 increased by a factor >10, whereas the NH_3 emissions increased by a factor of approximately 2. This is in
633 agreement with recent laboratory measurements that found that the release of NO_x is favoured during the
634 flaming stage and the release of reduced forms of nitrogen, such as NH_3, is favoured during the
635 smoldering phase (Roberts et al., 2020) (also see Fig. 4). However, the CFFEPS CO emission rates do

https://doi.org/10.5194/acp-2022-245
Preprint. Discussion started: 14 April 2022


Atmospheric Chemistry and Physics Discussions

not track the increase in CO emissions between the aircraft-derived value and the two TROPOMI values, indicating that the CO EF for flaming is low in the model. This highlights the need to validate model emission rates with measurements to adjust and update the EFs accordingly.

Using the aircraft- and satellite-derived emission rates relative to FRP (in units of t h^{-1} MW^{-1}) to represent the the two end burning states ie. smoldering and flaming conditions, estimates of total emissions from this fire were made for CO, NO_x and NH_3. Total emissions were estimated by integrating the GOES FRP over the period June 24, 2018 17:00 UTC to June 25 23:00 UTC, and applying the derived smoldering and flaming emission ratios. It was assumed that flaming occured for FRP >500 MW and smoldering for FRP < 500 MW. Emission rates were estimated with respect to the FRP for the flaming and smoldering phases of the fire. The CO emission rates are roughly twice as large during smoldering compared to flaming. For the satellite emission estimates from the two overpasses during the flaming phase of the fire, the CO emission rates are very similar and well within the uncertainties (19:00 UTC ER_{CO} = 4.7 t MW^{-1}; 2000 UTC ER_{CO} = 43 t MW^{-1}). The ratio for NO_x is also twice as large for flaming compared to smoldering, and for NH_3, the ratio is ~5 times larger for smoldering than flaming. Assuming that the fire went out when GOES did not observe any hot spots, total emissions for this fire of CO, NO_x and NH_3 are estimated at 21,808, 104.1, and 83.7 tonnes, respectively. If the fire is assumed to have continued burning when GOES did not detect any fire hot spots (between 22:00 - 04:00 UTC and 07:00 - 15:00 UTC, with an FRP of 150 MW (~GOES detection limit; Roberts et al., 2015), the emissions increase to 23,986, 106.4 and 97.7 tonnes, respectively, providing an upper limit of emissions. The combination of aircraft and satellite-derived emission estimates for multiple species helps to obtain the diurnal variability of emissions and to obtain more complete details on the emission information across different burning stages.

4. Summary and Implications

This study provides detailed emissions information for boreal forest wildfires under a smoldering combustion process. Highly speciated airborne measurements showed a large diversity of chemical classes highlighting the complexity of emissions. Despite extensive speciation across a range of NMOG

https://doi.org/10.5194/acp-2022-245
Preprint. Discussion started: 14 April 2022


Atmospheric Chemistry and Physics Discussions

662 volatilities, a substantial portion of $NMOG_T$ remained unidentified (46.4 %) and is expected to be
663 comprised of more highly functionalized VOCs and I/SVOCs. Although these compounds are
664 challenging to measure, their characterization is necessary to more fully understand particle-gas
665 partitioning processes related to the formation of SOA. Methodological advancements to achieve higher
666 time resolution speciated measurements of I/SIVOCs would move towards further $NMOG_T$ closure and
667 span a more complete range of volatilities. A detailed suite of EFs that were derived in this study can be
668 used to improve chemical speciation profiles that are relevant for air quality modelling of boreal forest
669 wildfires. Aircraft-derived emission estimates were paired with those from satellite observations
670 demonstrating their combined usefulness in assessing modelled emissions variability. As satellite
671 instrumentation and methodologies advance, linking emissions derived from aircraft (and ground)
672 observations for additional compounds will improve the ability to simulate and predict the diurnal
673 variation in wildfire emissions.
674 Although the measurements from this study provide a detailed characterization of a wildfire, the
675 results represent only one smoldering boreal forest wildfire. Additional measurements are needed under a
676 variety of fire conditions (combustion state, fire stage, biomass mixtures, time of day, etc) in order to
677 elucidate the major controlling factors and improve statistical representation for constraining and
678 modelling these sources. For example, measurements are needed to assess dark chemistry reactions in
679 biomass burning emissions which have been shown to be important in the formation of OA (Kodros et al.,
680 2020) and brown carbon (Palm et al.; 2020). In addition, reduced actinic flux associated with high
681 particle loadings in biomass burning emissions can influence plume chemistry (e.g. Juncosa-Calahorrano
682 et al., 2021; Parrington et al., 2013). The emissions information in this work will contribute to the
683 evaluation and improvements of models that are essential for reliable predictions of boreal forest wildfire
684 pollutants and their downwind chemistry.
685
686
687

https://doi.org/10.5194/acp-2022-245
Preprint. Discussion started: 14 April 2022


Atmospheric Chemistry and Physics Discussions

Acknowledgements

The authors acknowledge the significant technical and scientific contributions towards the success of this study from the AQRD technical and data teams, the NRC team, and excellent program management by Stewart Cober. JCD, MH, and DRG acknowledge support from the National Science Foundation (AGS1764126) and GERSTEL for their collaboration with the thermal desorption unit used as part of this study, and MH also acknowledges the Goldwater Scholarship Foundation. S.-M.L. acknowledges the support of the Ministry of Science and Technology of China (Grant 2019YFC0214700).

Author contribution

KH, SML, JL, MJW, JJBW, AL, PB, RLM, CM, AS, RMS, SM, AD, and MW all contributed to the collection and analyses of the aircraft observations in the field. JCD, MH, and DRG analysed the cartridge samples. ZO contributed to the analyses and created many of the figures. DT contributed to the analyses of the physical and combustion state of the wildfire fire. DG and EE provided the satellite observations and DG wrote the satellite comparison section. JC contributed to the comparisons with the model emission speciation profile. KH wrote the paper with input from all co-authors.

Competing interests

The authors declare that they have no substantive conflicts of interest, but acknowledge that DRG and JL are associate editors with Atmospheric Chemistry and Physics.

Data availability

All data used in this publication are available upon request.

https://doi.org/10.5194/acp-2022-245
Preprint. Discussion started: 14 April 2022


Atmospheric Chemistry and Physics Discussions

712 **References**

713 Adams, C., McLinden, C. A., Shephard, M. W., Dickson, N., Dammers, E., Chen, J., Makar, P., Cady-
714 Pereira, K. E., Tam, N., Kharol, S. K., Lamsal, L. N., and Krotkov, N. A.: Satellite-derived emissions of
715 carbon monoxide, ammonia, and nitrogen dioxide from the 2016 Horse River wildfire in the Fort
716 McMurray area, Atmos. Chem. Phys., 19, 2577-2599, https://doi.org/10.5194/acp-19-2577-2019, 2019.
717
718 Ahern, A. T., Robinson, E. S., Tkacik, D. S., Saleh, R., Hatch, L. E., Barsanti, K. C., Stockwell, C. E.,
719 Yokelson, R. J., Presto, A. A., Robinson, A. L., Sullivan, R. C., and Donahue, N. M.: Production of
720 secondary organic aerosol during aging of biomass burning smoke from fresh fuels and its relationship to
721 VOC Precursors, J. Geophys. Res.-Atmos, 124, 3583-3606, https://doi.org/10.1029/2018JD029068, 2019.
722
723 Akagi, S. K., Yokelson, R. J., Wiedinmyer, C., Alvarado, M. J., Reid, J. S., Karl, T., Crounse, J. D., and
724 Wennberg, P. O.: Emission factors for open and domestic biomass burning for use in atmospheric models,
725 Atmos. Chem. Phys., 11, 4039-4072, https://doi.org/10.5194/acp-11-4039-2011, 2011.
726
727 Akagi, S. K., Craven, J. S., Taylor, J. W., McMeeking, G. R., Yokelson, R. J., Burling, I. R., Urbanski, S.
728 P., Wold, C. E., Seinfeld, J. H., Coe, H., Alvarado, M. J., and Weise, D. R.: Evolution of trace gases and
729 particles emitted by a chaparral fire in California, Atmos. Chem. Phys., 12, 1397-1421,
730 https://doi.org/10.5194/acp-12-1397-2012, 2012.
731
732 Akagi, S. K., Yokelson, R. J., Burling, I. R., Meinardi, S., Simpson, I., Blake, D. R., McMeeking, G. R.,
733 Sullivan, A., Lee, T., Kreidenweis, S., Urbanski, S., Reardon, J., Griffith, D. W. T., Johnson, T. J., and
734 Weise, D. R.: Measurements of reactive trace gases and variable O3 formation rates in some South
735 Carolina biomass burning plumes, Atmos. Chem. Phys., 13, 1141-1165, https://doi.org/10.5194/acp-13-
736 1141-2013, 2013.
737
738 Alvarado, M. J., Logan, J. A., Mao, J., Apel, E., Riemer, D., Blake, D., Cohen, R. C., Min, K. E., Perring,
739 A. E., Browne, E. C., Wooldridge, P. J., Diskin, G. S., Sachse, G. W., Fuelberg, H., Sessions, W. R.,
740 Harrigan, D. L., Huey, G., Liao, J., Case-Hanks, A., Jimenez, J. L., Cubison, M. J., Vay, S. A.,
741 Weinheimer, A. J., Knapp, D. J., Montzka, D. D., Flocke, F. M., Pollack, I. B., Wennberg, P. O., Kurten,
742 A., Crounse, J., Clair, J. M. S., Wisthaler, A., Mikoviny, T., Yantosca, R. M., Carouge, C. C., and Le
743 Sager, P.: Nitrogen oxides and PAN in plumes from boreal fires during ARCTAS-B and their impact on
744 ozone: an integrated analysis of aircraft and satellite observations, Atmos. Chem. Phys., 10, 9739-9760,
745 https://doi.org/10.5194/acp-10-9739-2010, 2010.
746
747 Andreae, M. O.: Emission of trace gases and aerosols from biomass burning – an updated assessment,
748 Atmos. Chem. Phys., 19, 8523-8546, https://doi.org/10.5194/acp-19-8523-2019, 2019. Biomass burning
749 emission factors https://edmond.mpdl.mpg.de/imeji/collection/op2vVE8m0us_gcGC, ver 14 Apr 2021.
750
751 Andreae, M. O. and Merlet, P.: Emission of trace gases and aerosols from biomass burning, Global
752 Biogeochem. Cy., 15, 955-966, https://doi.org/10.1029/2000GB001382, 2001.
753
754 Baumgardner, D., Kok, G., and Raga, G.: Warming of the Arctic lower stratosphere by light absorbing
755 particles, Geophys. Res. Lett., 31, L06117, https://doi.org/10.1029/2003GL018883, 2004.
756
757 Bertschi, I., Yokelson, R. J., Ward, D. E., Babbitt, R. E., Susott, R. A., Goode, J. G., and Hao, W. M.:
758 Trace gas and particle emissions from fires in large diameter and belowground biomass fuels, J. Geophys.
759 Res.-Atmos, 108, 8472, https://doi.org/10.1029/2002JD002100, 2003.
760

https://doi.org/10.5194/acp-2022-245
Preprint. Discussion started: 14 April 2022

Atmospheric Chemistry and Physics Discussions

761 Bond-Lamberty, B., Gower, S. T., Wang, C., Cyr, P., and Veldhuis, H.: Nitrogen dynamics of a boreal
762 black spruce wildfire chronosequence, Biogeochemistry, 81, 1-16, https://doi.org/10.1007/s10533-006-
763 9025-7, 2006.
764
765 Bruns, E. A., El Haddad, I., Slowik, J. G., Kilic, D., Klein, F., Baltensperger, U., and Prevot, A. S. H.:
766 Identification of significant precursor gases of secondary organic aerosols from residential wood
767 combustion, Sci. Rep., 6, https://doi.org/10.1038/srep27881, 2016.
768
769 Burling, I. R., Yokelson, R. J., Akagi, S. K., Urbanski, S. P., Wold, C. E., Griffith, D. W. T., Johnson, T.
770 J., Reardon, J., and Weise, D. R.: Airborne and ground-based measurements of the trace gases and
771 particles emitted by prescribed fires in the United States, Atmos. Chem. Phys., 11, 12197-12216,
772 https://doi.org/10.5194/acp-11-12197-2011, 2011.
773
774 Bush, E. and Lemmen, D. S.: Canada's changing climate report, Government of Canada, Ottawa, ON.,
775 444 pp., www.ChangingClimate.ca/CCCR2019, 2019.
776
777 Campos, I., Abrantes, N., Pereira, P., Micaelo, A. C., Vale, C., and Keizer, J. J.: Forest fires as potential
778 triggers for production and mobilization of polycyclic aromatic hydrocarbons to the terrestrial ecosystem,
779 Land Degrad. Dev., 30, 2360-2370, https://doi.org/10.1002/ldr.3427, 2019.
780
781 Carter, W. P. L. and Heo, G.: Development of revised SAPRC aromatics mechanisms, Atmos. Environ.,
782 77, 404-414, https://doi.org/10.1016/j.atmosenv.2013.05.021, 2013.
783
784 Cascio, W. E.: Wildland fire smoke and human health, Sci. Total Environ., 624, 586-595,
785 https://doi.org/10.1016/j.scitotenv.2017.12.086, 2018.
786
787 Chen, J., Anderson, K., Pavlovic, R., Moran, M. D., Englefield, P., Thompson, D. K., Munoz-Alpizar, R.,
788 and Landry, H.: The FireWork v2.0 air quality forecast system with biomass burning emissions from the
789 Canadian Forest Fire Emissions Prediction System v2.03, Geosci. Model Dev., 12, 3283-3310,
790 https://doi.org/10.5194/gmd-12-3283-2019, 2019.
791
792 Cherry, N. and Haynes, W.: Effects of the Fort McMurray wildfires on the health of evacuated workers:
793 follow-up of 2 cohorts, Can. Med. Assoc. J., 5, E638-E645, https://doi.org/10.9778/cmajo.20170047,
794 2017.
795
796 Ciccioli, P., Centritto, M., and Loreto, F.: Biogenic volatile organic compound emissions from vegetation
797 fires, Plant, Cell Environ., 37, 1810-1825, https://doi.org/10.1111/pce.12336, 2014.
798
799 Coggon, M. M., Lim, C. Y., Koss, A. R., Sekimoto, K., Yuan, B., Gilman, J. B., Hagan, D. H., Selimovic,
800 V., Zarzana, K. J., Brown, S. S., Roberts, J. M., Müller, M., Yokelson, R., Wisthaler, A., Krechmer, J. E.,
801 Jimenez, J. L., Cappa, C., Kroll, J. H., de Gouw, J., and Warneke, C.: OH chemistry of non-methane
802 organic gases (NMOGs) emitted from laboratory and ambient biomass burning smoke: evaluating the
803 influence of furans and oxygenated aromatics on ozone and secondary NMOG formation, Atmos. Chem.
804 Phys., 19, 14875-14899, https://doi.org/10.5194/acp-19-14875-2019, 2019.
805
806 Cole, A. S., Steffen, A., Eckley, C. S., Narayan, J., Pilote, M., Tordon, R., Graydon, J. A., St. Louis, V.
807 L., Xu, X., and Branfireun, B. A.: A survey of mercury in air and precipitation across Canada: Patterns
808 and trends, Atmosphere, 5, 635-668, https://doi.org/10.3390/atmos5030635, 2014.
809
810 de Gouw, J. A., Warneke, C., Stohl, A., Wollny, A. G., Brock, C. A., Cooper, O. R., Holloway, J. S.,
811 Trainer, M., Fehsenfeld, F. C., Atlas, E. L., Donnelly, S. G., Stroud, V., and Lueb, A.: The VOC

composition of merged and aged forest fire plumes from Alaska and Western Canada, J. Geophys. Res.-Atmos, 111, D10303, https://doi.org/10.1029/2005JD006175, 2006.

de Groot, W. J., Pritchard, J. M., and Lynham, T. J.: Forest floor fuel consumption and carbon emissions in Canadian boreal forest fires, Can. J. Forest Res., 39, 367-382, https://doi.org/10.1139/x08-192, 2009.

Decker, Z. C. J., Zarzana, K. J., Coggon, M., Min, K.-E., Pollack, I., Ryerson, T. B., Peischl, J., Edwards, P., Dubé, W. P., Markovic, M. Z., Roberts, J. M., Veres, P. R., Graus, M., Warneke, C., de Gouw, J., Hatch, L. E., Barsanti, K. C., and Brown, S. S.: Nighttime chemical transformation in biomass burning plumes: A box model analysis Initialized with aircraft observations, Environ. Sci. Technol., 53, 2529-2538, https://doi.org/10.1021/acs.est.8b05359, 2019.

Decker, Z.C., Wang. S., Novel analysis to quantify plume crosswind heterogeneity applied to biomass burning smoke, EST, 2021.

Ditto, J. C., Joo, T., Slade, J. H., Shepson, P. B., Ng, N. L., and Gentner, D. R.: Nontargeted Tandem Mass Spectrometry Analysis Reveals Diversity and Variability in Aerosol Functional Groups across Multiple Sites, Seasons, and Times of Day, Environmental Science and Technology Letters, 7, 60-69, https://doi.org/10.1021/acs.estlett.9b00702, 2020.

Ditto, J. C., He, M., Hass-Mitchell, T. N., Moussa, S. G., Hayden, K., Li, S. M., Liggio, J., Leithead, A., Lee, P., Wheeler, M. J., Wentzell, J. J. B., and Gentner, D. R.: Atmospheric evolution of emissions from a boreal forest fire: the formation of highly functionalized oxygen-, nitrogen-, and sulfur-containing organic compounds, Atmos. Chem. Phys., 21, 255-267, https://doi.org/10.5194/acp-21-255-2021, 2021.

Ditto, J. C., Machesky, J., and Gentner, D. R.: Analysis of reduced and oxidized nitrogen-containing organic compounds at a coastal site in summer and winter, Atmos. Chem. Phys., 22, 3045-3065, https://doi.org/10.5194/acp-22-3045-2022, 2022.

Donahue, N. M., Epstein, S. A., Pandis, S. N., and Robinson, A. L.: A two-dimensional volatility basis set: 1. organic-aerosol mixing thermodynamics, Atmos. Chem. Phys., 11, 3303-3318, https://doi.org/10.5194/acp-11-3303-2011, 2011.

EPA: Air method, toxic organics-15 (TO-15): Compendium of methods for the determination of toxic organic compounds in ambient air, second edition: Determination of volatile organic compounds (VOCs) in air collected in specially-prepared canisters and analyzed by gas chromatography/mass spectrometry (GC/MS)." EPA 625/R-96/010b, 1999.

Finlay, S. E., Moffat, A., Gazzard, R., Baker, D., and Murray, V.: Health impacts of wildfires, PLoS Curr., 4, e4f959951cce959952c, https://doi.org/10.1371/4f959951cce2c, 2012.

Garofalo, L. A., Pothier, M. A., Levin, E. J. T., Campos, T., Kreidenweis, S. M., and Farmer, D. K.: Emission and evolution of submicron organic aerosol in smoke from wildfires in the Western United States, ACS Earth Space Chem., 3, 1237-1247, https://doi.org/10.1021/acsearthspacechem.9b00125, 2019.

Gilman, J. B., Lerner, B. M., Kuster, W. C., Goldan, P. D., Warneke, C., Veres, P. R., Roberts, J. M., de Gouw, J. A., Burling, I. R., and Yokelson, R. J.: Biomass burning emissions and potential air quality impacts of volatile organic compounds and other trace gases from fuels common in the US, Atmos. Chem. Phys., 15, 13915-13938, https://doi.org/10.5194/acp-15-13915-2015, 2015.

https://doi.org/10.5194/acp-2022-245
Preprint. Discussion started: 14 April 2022

Atmospheric Chemistry and Physics Discussions

Goode, J. G., Yokelson, R. J., Ward, D. E., Susott, R. A., Babbitt, R. E., Davies, M. A., and Hao, W. M.: Measurements of excess O_3, CO_2, CO, CH_4, C_2H_4, C_2H_2, HCN, NO, NH_3, HCOOH, CH_3COOH, HCHO, and CH_3OH in 1997 Alaskan biomass burning plumes by airborne fourier transform infrared spectroscopy (AFTIR), J. Geophys. Res., 105, 22147-22166, https://doi.org/10.1029/2000JD900287, 2000.

Gordon, M., Li, S. M., Staebler, R., Darlington, A., Hayden, K., O'Brien, J., and Wolde, M.: Determining air pollutant emission rates based on mass balance using airborne measurement data over the Alberta oil sands operations, Atmos. Meas. Tech., 8, 3745-3765, https://doi.org/10.5194/amt-8-3745-2015, 2015.

Griffin, D., McLinden, C. A., Dammers, E., Adams, C., Stockwell, C., Warneke, C., Bourgeois, I., Peischl, J., Ryerson, T. B., Zarzana, K. J., Rowe, J. P., Volkamer, R., Knote, C., Kille, N., Koenig, T. K., Lee, C. F., Rollins, D., Rickly, P. S., Chen, J., Fehr, L., Bourassa, A., Degenstein, D., Hayden, K., Mihele, C., Wren, S. N., Liggio, J., Akingunola, A., and Makar, P.: Biomass burning nitrogen dioxide emissions derived from space with TROPOMI: methodology and validation, Atmos. Meas. Tech. Discuss. [preprint], https://doi.org/10.5194/amt-2021-223, in review, 2021.

Griffith, D. W. T., Mankin, W. G., Coffey, M. T., Ward, D. E., and Riebau, A.: FTIR remote sensing of biomass burning emissions of CO_2, CO, CH_4, CH_2O, NO, NO_2, NH_3, and N_2O, in: Global Biomass Burning: Atmospheric, Climatic, and Biospheric Implications, edited by: Levine, J. S., MIT Press, Cambride, MA, United States, 230-241, 1991.

Guérette, E. A., Paton-Walsh, C., Desservettaz, M., Smith, T. E. L., Volkova, L., Weston, C. J., and Meyer, C. P.: Emissions of trace gases from Australian temperate forest fires: Emission factors and dependence on modified combustion efficiency, Atmos. Chem. Phys., 18, 3717-3735, https://doi.org/10.5194/acp-18-3717-2018, 2018.

Hatch, L. E., Luo, W., Pankow, J. F., Yokelson, R. J., Stockwell, C. E., and Barsanti, K. C.: Identification and quantification of gaseous organic compounds emitted from biomass burning using two-dimensional gas chromatography–time-of-flight mass spectrometry, Atmos. Chem. Phys., 15, 1865-1899, https://doi.org/10.5194/acp-15-1865-2015, 2015.

Hatch, L. E., Rivas-Ubach, A., Jen, C. N., Lipton, M., Goldstein, A. H., and Barsanti, K. C.: Measurements of I/SVOCs in biomass-burning smoke using solid-phase extraction disks and two-dimensional gas chromatography, Atmos. Chem. Phys., 18, 17801-17817, https://doi.org/10.5194/acp-18-17801-2018, 2018.

Hatch, L. E., Yokelson, R. J., Stockwell, C. E., Veres, P. R., Simpson, I. J., Blake, D. R., Orlando, J. J., and Barsanti, K. C.: Multi-instrument comparison and compilation of non-methane organic gas emissions from biomass burning and implications for smoke-derived secondary organic aerosol precursors, Atmos. Chem. Phys., 17, 1471-1489, https://doi.org/10.5194/acp-17-1471-2017, 2017.

Hatch, L. E., Jen, C. N., Kreisberg, N. M., Selimovic, V., Yokelson, R. J., Stamatis, C., York, R. A., Foster, D., Stephens, S. L., Goldstein, A. H., and Barsanti, K. C.: Highly speciated measurements of terpenoids emitted from laboratory and mixed-conifer forest prescribed fires, Environ. Sci. Technol., 53, 9418-9428, https://doi.org/10.1021/acs.est.9b02612, 2019.

Hecobian, A., Liu, Z., Hennigan, C. J., Huey, L. G., Jimenez, J. L., Cubison, M. J., Vay, S., Diskin, G. S., Sachse, G. W., Wisthaler, A., Mikoviny, T., Weinheimer, A. J., Liao, J., Knapp, D. J., Wennberg, P. O., Kürten, A., Crounse, J. D., Clair, J. S., Wang, Y., and Weber, R. J.: Comparison of chemical characteristics of 495 biomass burning plumes intercepted by the NASA DC-8 aircraft during the

ARCTAS/CARB-2008 field campaign, Atmos. Chem. Phys., 11, 13325-13337, https://doi.org/10.5194/acp-11-13325-2011, 2011.

Hodshire, A. L., Akherati, A., Alvarado, M. J., Brown-Steiner, B., Jathar, S. H., Jimenez, J. L., Kreidenweis, S. M., Lonsdale, C. R., Onasch, T. B., Ortega, A. M., and Pierce, J. R.: Aging effects on biomass burning aerosol mass and composition: A critical review of field and laboratory studies, Environ. Sci. Technol., 53, 10007-10022, https://doi.org/10.1021/acs.est.9b02588, 2019.

Jia, Y., Yu, G., Gao, Y., He, N., Wang, Q., Jiao, C., and Zuo, Y.: Global inorganic nitrogen dry deposition inferred from ground- and space-based measurements, Sci. Rep., 6, 19810, https://doi.org/10.1038/srep19810, 2016.

Johnstone, J. F., Hollingsworth, T. N., Chapin III, F. S., and Mack, M. C.: Changes in fire regime break the legacy lock on successional trajectories in Alaskan boreal forest, Global Change Biol., 16, 1281-1295, https://doi.org/10.1111/j.1365-2486.2009.02051.x, 2010.

Juncosa Calahorrano, J. F., Lindaas, J., O'Dell, K., Palm, B. B., Peng, Q., Flocke, F., Pollack, I. B., Garofalo, L. A., Farmer, D. K., Pierce, J. R., Collett Jr., J. L., Weinheimer, A., Campos, T., Hornbrook, R. S., Hall, S. R., Ullmann, K., Pothier, M. A., Apel, E. C., Permar, W., Hu, L., Hills, A. J., Montzka, D., Tyndall, G., Thornton, J. A., and Fischer, E. V.: Daytime oxidized reactive nitrogen partitioning in western U.S. wildfire smoke plumes, J. Geophys. Res.-Atmos, 126, e2020JD033484, https://doi.org/10.1029/2020JD033484, 2021.

Kaiser, J. W., Heil, A., Andreae, M. O., Benedetti, A., Chubarova, N., Jones, L., Morcrette, J.-J., Razinger, M., Schultz, M. G., Suttie, M., and van der Werf, G. R.: Biomass burning emissions estimated with a global fire assimilation system based on observed fire radiative power, Biogeosciences, 9, 527–554, https://doi.org/10.5194/bg-9-527-2012, 2012.

Kallenborn, R., Halsall, C., Dellong, M., and Carlsson, P.: The influence of climate change on the global distribution and fate processes of anthropogenic persistent organic pollutants, J. Environ. Monitor., 14, 2854-2869, https://doi.org/10.1039/c2em30519d, 2012.

Khare, P., Marcotte, A., Sheu, R., Walsh, A. N., Ditto, J. C., and Gentner, D. R.: Advances in offline approaches for trace measurements of complex organic compound mixtures via soft ionization and high-resolution tandem mass spectrometry, J. Chromatogr. A, 1598, 163-174, https://doi.org/10.1016/j.chroma.2019.03.037, 2019.

Kodros, J. K., Papanastasiou, D. K., Paglione, M., Masiol, M., Squizzato, S., Florou, K., Skyllakou, K., Kaltsonoudis, C., Nenes, A., and Pandis, S. N.: Rapid dark aging of biomass burning as an overlooked source of oxidized organic aerosol, P. Natl. Acad. Sci. USA, 117, 33028-33033, https://doi.org/10.1073/pnas.2010365117, 2020.

Kondo, Y., Sahu, L., Moteki, N., Khan, F., Takegawa, N., Liu, X., Koike, M., and Miyakawa, T.: Consistency and traceability of black carbon measurements made by laser-induced incandescence, thermal-optical transmittance, and filter-based photo-absorption techniques, Aerosol Sci. Tech., 45, 295-312, https://doi.org/10.1080/02786826.2010.533215, 2011.

Koss, A. R., Sekimoto, K., Gilman, J. B., Selimovic, V., Coggon, M. M., Zarzana, K. J., Yuan, B., Lerner, B. M., Brown, S. S., Jimenez, J. L., Krechmer, J., Roberts, J. M., Warneke, C., Yokelson, R. J., and de Gouw, J.: Non-methane organic gas emissions from biomass burning: identification,

963 quantification, and emission factors from PTR-ToF during the FIREX 2016 laboratory experiment,
964 Atmos. Chem. Phys., 18, 3299-3319, https://doi.org/10.5194/acp-18-3299-2018, 2018.
965
966 Kotchenruther, R. A. and Hobbs, P. V.: Humidification factors of aerosols from biomass burning in
967 Brazil, J. Geophys. Res.-Atmos, 103, 32081-32089, https://doi.org/10.1029/98JD00340, 1998.
968
969 Kou-Giesbrecht, S. and Menge, D.: Nitrogen-fixing trees could exacerbate climate change under elevated
970 nitrogen deposition, Nat. Commun., 10, 1493, https://doi.org/10.1038/s41467-019-09424-2, 2019.
971
972 Kumar, V., Chandra, B. P., and Sinha, V.: Large unexplained suite of chemically reactive compounds
973 present in ambient air due to biomass fires, Sci. Rep., 8, 626, https://doi.org/10.1038/s41598-017-19139-
974 3, 2018.
975
976 Laborde, M., Mertes, P., Zieger, P., Dommen, J., Baltensperger, U., and Gysel, M.: Sensitivity of the
977 Single Particle Soot Photometer to different black carbon types, Atmos. Meas. Tech., 5, 1031-1043,
978 https://doi.org/10.5194/amt-5-1031-2012, 2012.
979
980 Landis, M. S., Edgerton, E. S., White, E. M., Wentworth, G. R., Sullivan, A. P., and Dillner, A. M.: The
981 impact of the 2016 Fort McMurray Horse River Wildfire on ambient air pollution levels in the Athabasca
982 Oil Sands Region, Alberta, Canada, Sci. Total Environ., 618, 1665-1676,
983 https://doi.org/10.1016/j.scitotenv.2017.10.008, 2018.
984
985 Lapina, K., Honrath, R. E., Owen, R. C., Val Martin, M., Hyer, E. J., and Fialho, P.: Late summer
986 changes in burning conditions in the boreal regions and their implications for NOx and CO emissions
987 from boreal fires, J. Geophys. Res., 113, D11304, https://doi.org/10.1029/2007JD009421, 2008.
988
989 Lee, T., Sullivan, A. P., Mack, L., Jimenez, J. L., Kreidenweis, S. M., Onasch, T. B., Worsnop, D. R.,
990 Malm, W., Wold, C. E., Hao, W. M., and Collett Jr, J. L.: Chemical smoke marker emissions during
991 flaming and smoldering phases of laboratory open burning of wildland fuels, Aerosol Sci. Tech., 44, i-v,
992 https://doi.org/10.1080/02786826.2010.499884, 2010.
993
994 Leifer, I., Melton, C. Tratt, D.M., Buckland, K.N., Clarisse, L., Coheur, P., Frash, J., Gupta, M., Johnson,
995 P.D., Leen, J.B., Van Damme, M., Whitburn, S., and Yurganov, L.: Remote sensing and in situ
996 measurements of methane and ammonia emissions from a megacity dairy complex: Chino, CA, Environ.
997 Poll., 221, 37-51, https://doi.org/10.1016/j.envpol.2016.09.083, 2017.
998
999 Lerner, B. M., Gilman, J. B., Aikin, K. C., Atlas, E. L., Goldan, P. D., Graus, M., Hendershot, R.,
1000 Isaacman-VanWertz, G. A., Koss, A., Kuster, W. C., Lueb, R. A., McLaughlin, R. J., Peischl, J., Sueper,
1001 D., Ryerson, T. B., Tokarek, T. W., Warneke, C., Yuan, B., and de Gouw, J. A.: An improved, automated
1002 whole air sampler and gas chromatography mass spectrometry analysis system for volatile organic
1003 compounds in the atmosphere, Atmos. Meas. Tech., 10, 291-313, https://doi.org/10.5194/amt-10-291-
1004 2017, 2017.
1005
1006 Li, K., Liggio, J., Han, C., Liu, Q., Moussa, S. G., Lee, P., and Li, S.-M.: Understanding the impact of
1007 high-NOx conditions on the formation of secondary organic aerosol in the photooxidation of oil sand-
1008 related precursors, Environ. Sci. Technol., 53, 14420-14429, https://doi.org/10.1021/acs.est.9b05404,
1009 2019.
1010
1011 Li, K., Wentzell, J. J. B., Liu, Q., Leithead, A., Moussa, S. G., Wheeler, M. J., Han, C., Lee, P., Li, S.-M.,
1012 and Liggio, J.: Evolution of atmospheric total organic carbon from petrochemical mixtures, Environ. Sci.
1013 Technol., 55, 12841-12851, https://doi.org/10.1021/acs.est.1c02620, 2021.

https://doi.org/10.5194/acp-2022-245
Preprint. Discussion started: 14 April 2022

Atmospheric Chemistry and Physics Discussions

Li, S.-M., Leithead, A., Moussa, S. G., Liggio, J., Moran, M. D., Wang, D., Hayden, K., Darlington, A., Gordon, M., Staebler, R., Makar, P. A., Stroud, C. A., McLaren, R., Liu, P. S. K., O'Brien, J., Mittermeier, R. L., Zhang, J., Marson, G., Cober, S. G., Wolde, M., and Wentzell, J. J. B.: Differences between measured and reported volatile organic compound emissions from oil sands facilities in Alberta, Canada, P. Natl. Acad. Sci. USA, 114, E3756-E3765, https://doi.org/10.1073/pnas.1617862114, 2017.

Li, Y., Poschl, U., and Shiraiwa, M.: Molecular corridors and parameterizations of volatility in the chemical evolution of organic aerosols, Atmos. Chem. Phys., 16, 3327-3344, https://doi.org/10.5194/acp-16-3327-2016, 2016.

Lindaas, J., Pollack, I. B., Garofalo, L. A., Pothier, M. A., Farmer, D. K., Kreidenweis, S. M., Campos, T. L., Flocke, F., Weinheimer, A. J., Montzka, D. D., Tyndall, G. S., Palm, B. B., Peng, Q., Thornton, J. A., Permar, W., Wielgasz, C., Hu, L., Ottmar, R. D., Restaino, J. C., Hudak, A. T., Ku, I.-T., Zhou, Y., Sive, B. C., Sullivan, A., Collett Jr, J. L., and Fischer, E. V.: Emissions of reactive nitrogen from western U.S. wildfires during summer 2018, J. Geophys. Res.-Atmos, 125, e2020JD032657, https://doi.org/10.1029/2020JD032657, 2020.

Liu, Y., Liggio, J., Hayden, K., Mihele, C., Wentzell, J., Darlington, A., Moussa, S., Huang, Y., Xie, C., Yang, Y., Zhang, Y., Han, T., Wolde, M., and Li, S.-M.: Quantifying the interplay of physical and chemical evolution of oxidized reactive nitrogen in a boreal forest fire plume using airborne measurements, in preparation for submission to ES&T, 2022.

Liu, X., Huey, L. G., Yokelson, R. J., Selimovic, V., Simpson, I. J., Müller, M., Jimenez, J. L., Campuzano-Jost, P., Beyersdorf, A. J., Blake, D. R., Butterfield, Z., Choi, Y., Crounse, J. D., Day, D. A., Diskin, G. S., Dubey, M. K., Fortner, E., Hanisco, T. F., Hu, W., King, L. E., Kleinman, L., Meinardi, S., Mikoviny, T., Onasch, T. B., Palm, B. B., Peischl, J., Pollack, I. B., Ryerson, T. B., Sachse, G. W., Sedlacek, A. J., Shilling, J. E., Springston, S., St. Clair, J. M., Tanner, D. J., Teng, A. P., Wennberg, P. O., Wisthaler, A., and Wolfe, G. M.: Airborne measurements of western U.S. wildfire emissions: Comparison with prescribed burning and air quality implications, J. Geophys. Res.-Atmos., 122, 6108-6129, https://doi.org/10.1002/2016JD026315, 2017.

Loehman, R. A., Reinhardt, E., and Riley, K. L.: Wildland fire emissions, carbon, and climate: Seeing the forest and the trees – A cross-scale assessment of wildfire and carbon dynamics in fire-prone, forested ecosystems, For. Ecol. Manag., 317, 9-19, https://doi.org/10.1016/j.foreco.2013.04.014, 2014.

Matz, C.J., Egyed, M., Xi, G., Racine, J., Pavlovic, R., Rittmaster, R., Henderson, S.B., and Stieb, D.M.: Health impact analysis of $PM_{2.5}$ from wildfire smoke in Canada (2013-2015, 2017-2018), Sci. Total Environ., 725(10), https://doi.org/10.1016/j.scitotenv.2020.138506, 2020.

May, A. A., McMeeking, G. R., Lee, T., Taylor, J. W., Craven, J. S., Burling, I., Sullivan, A. P., Akagi, S., Collett Jr., J. L., Flynn, M., Coe, H., Urbanski, S. P., Seinfeld, J. H., Yokelson, R. J., and Kreidenweis, S. M.: Aerosol emissions from prescribed fires in the United States: A synthesis of laboratory and aircraft measurements, J. Geophys. Res.-Atmos, 119, 11826-11849, https://doi.org/10.1002/2014JD021848, 2014.

McGee, T., McFarlane, B., and Tymstra, C.: Chapter 3 - Wildfire: A Canadian Perspective, in: Wildfire Hazards, Risks and Disasters, edited by: Shroder, J. F., and Paton, D., Elsevier, Amsterdam, The Netherlands, 35-58, https://doi.org/10.1016/B978-0-12-410434-1.00003-8, 2015.

1064 McLagan, D. S., Stupple, G. W., Darlington, A., Hayden, K., and Steffen, A.: Where there is smoke there
1065 is mercury: Assessing boreal forest fire mercury emissions using aircraft and highlighting uncertainties
1066 associated with upscaling emissions estimates, Atmos. Chem. Phys., 21, 5635-5653,
1067 https://doi.org/10.5194/acp-21-5635-2021, 2021.
1068
1069 McMeeking, G. R., Kreidenweis, S. M., Baker, S., Carrico, C. M., Chow, J. C., Collett Jr., J. L., Hao, W.
1070 M., Holden, A. S., Kirchstetter, T. W., Malm, W. C., Moosmüller, H., Sullivan, A. P., and Wold, C. E.:
1071 Emissions of trace gases and aerosols during the open combustion of biomass in the laboratory, J.
1072 Geophys. Res.-Atmos, 114, D19210, https://doi.org/10.1029/2009JD011836, 2009.
1073
1074 Miller, D. J., Sun, K., Zondlo, M. A., Kanter, D., Dubovik, O., Welton, E. J., Winker, D. M., and Ginoux,
1075 P.: Assessing boreal forest fire smoke aerosol impacts on U.S. air quality: A case study using multiple
1076 data sets, J. Geophys. Res.-Atmos, 116, D22209, https://doi.org/10.1029/2011JD016170, 2011.
1077
1078 Moteki, N. and Kondo, Y.: Dependence of laser-induced incandescence on physical properties of black
1079 carbon aerosols: Measurements and theoretical interpretation, Aerosol Sci. Tech., 44, 663-675,
1080 https://doi.org/10.1080/02786826.2010.484450, 2010.
1081
1082 Moussa, S. G., Leithead, A., Li, S. M., Chan, T. W., Wentzell, J. J. B., Stroud, C., Zhang, J. H., Lee, P.,
1083 Lu, G., Brook, J. R., Hayden, K., Narayan, J., and Liggio, J.: Emissions of hydrogen cyanide from on-
1084 road gasoline and diesel vehicles, Atmos. Environ., 131, 185-195,
1085 https://doi.org/10.1016/j.atmosenv.2016.01.050, 2016.
1086
1087 NRCan, Blueprint for wildland fire science in Canada (2019-2029), Sankey, S., Technical
1088 Coordinator. Canadian Forest Service, Northern Forestry Centre, Edmonton, AB, 45p,
1089 https://cfs.nrcan.gc.ca/publications?id=39429, 2018.
1090
1091 O'Brien, J. J., Loudermilk, E. L., Hornsby, B. S., Hudak, A. T., Bright, B. C., Dickinson, M. B., Hiers, J.
1092 K., Teske, C., and Ottmar, R. D.: High-resolution infrared thermography for capturing wildland fire
1093 behaviour: RxCADRE 2012, Int. J. Wildland Fire, 25, 62-75, https://doi.org/10.1071/WF14165, 2015.
1094
1095 Palm, B. B., Peng, Q., Fredrickson, C. D., Lee, B. H., Garofalo, L. A., Pothier, M. A., Kreidenweis, S.
1096 M., Farmer, D. K., Pokhrel, R. P., Shen, Y., Murphy, S. M., Permar, W., Hu, L., Campos, T. L., Hall, S.
1097 R., Ullmann, K., Zhang, X., Flocke, F., Fischer, E. V., and Thornton, J. A.: Quantification of organic
1098 aerosol and brown carbon evolution in fresh wildfire plumes, P. Natl. Acad. Sci. USA, 117, 29469-29477,
1099 https://doi.org/10.1073/pnas.2012218117, 2020.
1100
1101 Peng, Q., Palm, B. B., Melander, K. E., Lee, B. H., Hall, S. R., Ullmann, K., Campos, T., Weinheimer, A.
1102 J., Apel, E. C., Hornbrook, R. S., Hills, A. J., Montzka, D. D., Flocke, F., Hu, L., Permar, W., Wielgasz,
1103 C., Lindaas, J., Pollack, I. B., Fischer, E. V., Bertram, T. H., and Thornton, J. A.: HONO Emissions from
1104 Western U.S. Wildfires Provide Dominant Radical Source in Fresh Wildfire Smoke, Environ. Sci.
1105 Technol., 54, 5954-5963, https://doi.org/10.1021/acs.est.0c00126, 2020.
1106
1107 Permar, W., Wang, Q., Selimovic, V., Wielgasz, C., Yokelson, R. J., Hornbrook, R. S., Hills, A. J., Apel,
1108 E. C., Ku, I.-T., Zhou, Y., Sive, B. C., Sullivan, A. P., Collett Jr, J. L., Campos, T. L., Palm, B. B., Peng,
1109 Q., Thornton, J. A., Garofalo, L. A., Farmer, D. K., Kreidenweis, S. M., Levin, E. J. T., DeMott, P. J.,
1110 Flocke, F., Fischer, E. V., and Hu, L.: Emissions of trace organic gases from western U.S. wildfires based
1111 on WE-CAN aircraft measurements, J. Geophys. Res.-Atmos, 126, e2020JD033838,
1112 https://doi.org/10.1029/2020JD033838, 2021.
1113

Randerson, J. T., Liu, H., Flanner, M. G., Chambers, S. D., Jin, Y., Hess, P. G., Pfister, G., Mack, M. C., Treseder, K. K., Welp, L. R., Chapin, F. S., Harden, J. W., Goulden, M. L., Lyons, E., Neff, J. C., Schuur, E. A., and Zender, C. S.: The impact of boreal forest fire on climate warming, Science, 314, 1130-1132, https://doi.org/10.1126/science.1132075, 2006.

Reid, C. E., Brauer, M., Johnston, F. H., Jerrett, M., Balmes, J. R., and Elliott, C. T.: Critical review of health impacts of wildfire smoke exposure, Environ. Health Persp., 124, 1334-1343, https://doi.org/10.1289/ehp.1409277, 2016.

Reid, J. S., Koppmann, R., Eck, T. F., and Eleuterio, D. P.: A review of biomass burning emissions part II: intensive physical properties of biomass burning particles, Atmos. Chem. Phys., 5, 799-825, https://doi.org/10.5194/acp-5-799-2005, 2005.

Roberts, J. M., Stockwell, C. E., Yokelson, R. J., de Gouw, J., Liu, Y., Selimovic, V., Koss, A. R., Sekimoto, K., Coggon, M. M., Yuan, B., Zarzana, K. J., Brown, S. S., Santin, C., Doerr, S. H., and Warneke, C.: The nitrogen budget of laboratory-simulated western US wildfires during the FIREX 2016 Fire Lab study, Atmos. Chem. Phys., 20, 8807-8826, https://doi.org/10.5194/acp-20-8807-2020, 2020.

Roberts, G., Wooster, M. J., Xu, W., Freeborn, P. H., Morcrette, J. J., Jones, L., Benedetti, A., Jiangping, H., Fisher, D., and Kaiser, J. W.: LSA SAF Meteosat FRP products – Part 2: Evaluation and demonstration for use in the Copernicus Atmosphere Monitoring Service (CAMS), Atmos. Chem. Phys., 15, 13241-13267, https://doi.org/10.5194/acp-15-13241-2015, 2015.

Rogers, C. F., Hudson, J. G., Hallett, J., and Penner, J. E.: Cloud Droplet Nucleation by Crude-Oil Smoke and Coagulated Crude-Oil Wood Smoke Particles, Atmos. Environ. a-Gen, 25, 2571-2580, https://doi.org/10.1016/0960-1686(91)90174-6, 1991.

Rogers, H. M., Ditto, J. C., and Gentner, D. R.: Evidence for impacts on surface-level air quality in the northeastern US from long-distance transport of smoke from North American fires during the Long Island Sound Tropospheric Ozone Study (LISTOS) 2018, Atmos. Chem. Phys., 20, 671-682, https://doi.org/10.5194/acp-20-671-2020, 2020.

Schwarz, J. P., Gao, R. S., Fahey, D. W., Thomson, D. S., Watts, L. A., Wilson, J. C., Reeves, J. M., Darbeheshti, M., Baumgardner, D. G., Kok, G. L., Chung, S. H., Schulz, M., Hendricks, J., Lauer, A., Kärcher, B., Slowik, J. G., Rosenlof, K. H., Thompson, T. L., Langford, A. O., Loewenstein, M., and Aikin, K. C.: Single-particle measurements of midlatitude black carbon and light-scattering aerosols from the boundary layer to the lower stratosphere, J. Geophys. Res.-Atmos, 111, D16207, https://doi.org/10.1029/2006JD007076, 2006.

Seidl, R., Thom, D., Kautz, M., Martin-Benito, D., Peltoniemi, M., Vacchiano, G., Wild, J., Ascoli, D., Petr, M., Honkaniemi, J., Lexer, M. J., Trotsiuk, V., Mairota, P., Svoboda, M., Fabrika, M., Nagel, T. A., and Reyer, C. P. O.: Forest disturbances under climate change, Nat. Clim. Change, 7, 395-402, https://doi.org/10.1038/nclimate3303, 2017.

Seinfeld, J. H. and Pandis, S. N.: Atmospheric chemistry and physics: from air pollution to climate change, John Wiley & Sons, New York, 1998.

Sekimoto, K., Li, S.-M., Yuan, B., Koss, A., Coggon, M., Warneke, C., and de Gouw, J.: Calculation of the sensitivity of proton-transfer-reaction mass spectrometry (PTR-MS) for organic trace gases using molecular properties, Int. J. Mass Spectrom., 421, 71-94, https://doi.org/10.1016/j.ijms.2017.04.006, 2017.

https://doi.org/10.5194/acp-2022-245
Preprint. Discussion started: 14 April 2022

Atmospheric Chemistry and Physics Discussions

Sheu, R., Marcotte, A., Khare, P., Charan, S., Ditto, J. C., and Gentner, D. R.: Advances in offline approaches for chemically speciated measurements of trace gas-phase organic compounds via adsorbent tubes in an integrated sampling-to-analysis system, J. Chromatogr. A, 1575, 80-90, https://doi.org/10.1016/j.chroma.2018.09.014, 2018.

Simoneit, B. R. T., Schauer, J. J., Nolte, C. G., Oros, D. R., Elias, V. O., Fraser, M. P., Rogge, W. F., and Cass, G. R.: Levoglucosan, a tracer for cellulose in biomass burning and atmospheric particles, Atmos. Environ., 33, 173-182, https://doi.org/10.1016/S1352-2310(98)00145-9, 1999.

Simpson, I. J., Akagi, S. K., Barletta, B., Blake, N. J., Choi, Y., Diskin, G. S., Fried, A., Fuelberg, H. E., Meinardi, S., Rowland, F. S., Vay, S. A., Weinheimer, A. J., Wennberg, P. O., Wiebring, P., Wisthaler, A., Yang, M., Yokelson, R. J., and Blake, D. R.: Boreal forest fire emissions in fresh Canadian smoke plumes: C_1-C_{10} volatile organic compounds (VOCs), CO_2, CO, NO_2, NO, HCN and CH_3CN, Atmos. Chem. Phys., 11, 6445-6463, https://doi.org/10.5194/acp-11-6445-2011, 2011.

Singh, H. B., Anderson, B. E., Brune, W. H., Cai, C., Cohen, R. C., Crawford, J. H., Cubison, M. J., Czech, E. P., Emmons, L., Fuelberg, H. E., Huey, G., Jacob, D. J., Jimenez, J. L., Kaduwela, A., Kondo, Y., Mao, J., Olson, J. R., Sachse, G. W., Vay, S. A., Weinheimer, A., Wennberg, P. O., and Wisthaler, A.: Pollution influences on atmospheric composition and chemistry at high northern latitudes: Boreal and California forest fire emissions, Atmos. Environ., 44, 4553-4564, https://doi.org/10.1016/j.atmosenv.2010.08.026, 2010.

Stephens, M., Turner, N., and Sandberg, J.: Particle identification by laser-induced incandescence in a solid-state laser cavity, Appl. Optics, 42, 3726-3736, https://doi.org/10.1364/ao.42.003726, 2003.

Stockwell, C. E., Veres, P. R., Williams, J., and Yokelson, R. J.: Characterization of biomass burning emissions from cooking fires, peat, crop residue, and other fuels with high-resolution proton-transfer-reaction time-of-flight mass spectrometry, Atmos. Chem. Phys., 15, 845-865, https://doi.org/10.5194/acp-15-845-2015, 2015.

Stockwell, C. E., Kupc, A., Witkowski, B., Talukdar, R. K., Liu, Y., Selimovic, V., Zarzana, K. J., Sekimoto, K., Warneke, C., Washenfelder, R. A., Yokelson, R. J., Middlebrook, A. M., and Roberts, J. M.: Characterization of a catalyst-based conversion technique to measure total particulate nitrogen and organic carbon and comparison to a particle mass measurement instrument, Atmos. Meas. Tech., 11, 2749-2768, https://doi.org/10.5194/amt-11-2749-2018, 2018.

Stockwell, C. E., Bela, M., Coggon, M. M., Gkatzelis, G. I., Wiggins, E. B., Gargulinski, E. M., Shingler, T., Fenn, M., Griffin, D., Holmes, C. D., Ye, X., Saide, P. E., Bourgeois, I., Peischl, J., Womack, C. C., Washenfelder, R. A., Veres, P. R., Neuman, J. A., Gilman, J. B., Lamplugh, A., Schwantes, R. H., McKeen, S. A., Wisthaler, A., Piel, F., Guo, H., Campuzano-Jost, P., Jimenez, J. L., Fried, A., Hanisco, T. F., Huey, L. G., Kondragunta, S., Zhang, X., Perring, A., Katich, J. M., Diskin, G. S., Nowak, J. B., Bui, T. P., Halliday, H. S., Pereira, G., James, E. P., Ahmadov, R., McLinden, C. A., Soja, A. J., Moore, R. H., Hair, J. W., and Warneke, C.: Airborne emission rate measurements validate remote sensing observations and emission inventories of western U.S. wildfires, submitted to ES&T, in review, 2021.

Urbanski, S.: Wildland fire emissions, carbon, and climate: Emission factors, For. Ecol. Manag., 317, 51-60, https://doi.org/10.1016/j.foreco.2013.05.045, 2014.

1214 Urbanski, S. P.: Combustion efficiency and emission factors for wildfire-season fires in mixed conifer
1215 forests of the Northern Rocky Mountains, US, Atmos. Chem. Phys., 13, 7241-7262,
1216 https://doi.org/10.5194/acp-13-7241-2013, 2013.
1217
1218 Urbanski, S. P., Hao, W. M., and Baker, S.: Chapter 4 Chemical Composition of Wildland Fire
1219 Emissions, in: Developments in Environmental Science, edited by: Bytnerowicz, A., Arbaugh, M. J.,
1220 Riebau, A. R., and Andersen, C., Elsevier, Amsterdam, The Netherlands, 79-107,
1221 https://doi.org/10.1016/S1474-8177(08)00004-1, 2009.
1222
1223 Uresk, D. W., Cline, J. F., and Rickard, W. H.: Growth rates of a cheatgrass community and some
1224 associated factors, J. Range Manage., 32, 168-170, https://doi.org/10.2307/3897114, 1979.
1225
1226 US EPA, SPECIATE Version 4.5 Database Development Documentation, Final Report EPA/600/R-
1227 16/294, September 2016. Available https://www.epa.gov/air-emissions-modeling/speciate.
1228
1229 van der Werf, G. R., Randerson, J. T., Giglio, L., Collatz, G. J., Kasibhatla, P. S., and Arellano Jr, A. F.:
1230 Interannual variability in global biomass burning emissions from 1997 to 2004, Atmos. Chem. Phys., 6,
1231 3423-3441, https://doi.org/10.5194/acp-6-3423-2006, 2006.
1232
1233 van der Werf, G. R., Randerson, J. T., Giglio, L., van Leeuwen, T. T., Chen, Y., Rogers, B. M., Mu, M.,
1234 van Marle, M. J. E., Morton, D. C., Collatz, G. J., Yokelson, R. J., and Kasibhatla, P. S.: Global fire
1235 emissions estimates during 1997–2016, Earth Syst. Sci. Data, 9, 697–720, https://doi.org/10.5194/essd-9-
1236 697-2017, 2017.
1237
1238 Veres, P., Roberts, J. M., Burling, I. R., Warneke, C., de Gouw, J., and Yokelson, R. J.: Measurements of
1239 gas-phase inorganic and organic acids from biomass fires by negative-ion proton-transfer chemical-
1240 ionization mass spectrometry, J. Geophys. Res.-Atmos, 115, D23302,
1241 https://doi.org/10.1029/2010JD014033, 2010.
1242
1243 Ward, D. E. and Radke, L. F.: Emissions measurements from vegetation fires: A comparative evaluation
1244 of methods and results, in: Fire in the Environment: The Ecological, Atmospheric, and Climatic
1245 Importance of Vegetation Fires. Dahlem Workshop Reports: Environmental Sciences Research Report
1246 13, edited by: Crutzen, P. J., and Goldammer, J. G., John Wiley & Sons, Chischester, England, 53-76,
1247 1993.
1248
1249 Whitman, E., Parisien, M. A., Thompson, D. K., and Flannigan, M. D.: Short-interval wildfire and
1250 drought overwhelm boreal forest resilience, Sci. Rep., 9, 18796, https://doi.org/10.1038/s41598-019-
1251 55036-7, 2019.
1252
1253 Wiggins, E. B., Andrews, A., Sweeney, C., Miller, J. B., Miller, C. E., Veraverbeke, S., Commane, R.,
1254 Wofsy, S., Henderson, J. M., and Randerson, J. T.: Boreal forest fire CO and CH_4 emission factors
1255 derived from tower observations in Alaska during the extreme fire season of 2015, Atmos. Chem. Phys.,
1256 21, 8557-8574, https://doi.org/10.5194/acp-21-8557-2021, 2021.
1257
1258 Wiggins, E. B., Soja, A. J., Gargulinski, E., Halliday, H. S., Pierce, R. B., Schmidt, C. C., Nowak, J. B.,
1259 DiGangi, J. P., Diskin, G. S., Katich, J. M., Perring, A. E., Schwarz, J. P., Anderson, B. E., Chen, G.,
1260 Crosbie, E. C., Jordan, C., Robinson, C. E., Sanchez, K. J., Shingler, T. J., Shook, M., Thornhill, K. L.,
1261 Winstead, E. L., Ziemba, L. D., and Moore, R. H.: High Temporal Resolution Satellite Observations of
1262 Fire Radiative Power Reveal Link Between Fire Behavior and Aerosol and Gas Emissions, Geophys. Res.
1263 Lett., 47, https://doi.org/10.1029/2020GL090707, 2020.
1264

https://doi.org/10.5194/acp-2022-245
Preprint. Discussion started: 14 April 2022

Atmospheric Chemistry and Physics Discussions

Wotton, B. M., Nock, C. A., and Flannigan, M. D.: Forest fire occurrence and climate change in Canada, Int. J. Wildland Fire, 19, 253-271, https://doi.org/10.1071/WF09002, 2010.

Yokelson, R. J., Bertschi, I. T., Christian, T. J., Hobbs, P. V., Ward, D. E., and Hao, W. M.: Trace gas measurements in nascent, aged, and cloud-processed smoke from African savanna fires by airborne Fourier transform infrared spectroscopy (AFTIR), J. Geophys. Res.-Atmos, 108, 8478, https://doi.org/10.1029/2002JD002322, 2003.

Yokelson, R. J., Burling, I. R., Gilman, J. B., Warneke, C., Stockwell, C. E., de Gouw, J., Akagi, S. K., Urbanski, S. P., Veres, P., Roberts, J. M., Kuster, W. C., Reardon, J., Griffith, D. W. T., Johnson, T. J., Hosseini, S., Miller, J. W., Cocker, D. R., Jung, H., and Weise, D. R.: Coupling field and laboratory measurements to estimate the emission factors of identified and unidentified trace gases for prescribed fires, Atmos. Chem. Phys., 13, 89-116, https://doi.org/10.5194/acp-13-89-2013, 2013.

Yokelson, R. J., Crounse, J. D., DeCarlo, P. F., Karl, T., Urbanski, S., Atlas, E., Campos, T., Shinozuka, Y., Kapustin, V., Clarke, A. D., Weinheimer, A., Knapp, D. J., Montzka, D. D., Holloway, J., Weibring, P., Flocke, F., Zheng, W., Toohey, D., Wennberg, P. O., Wiedinmyer, C., Mauldin, L., Fried, A., Richter, D., Walega, J., Jimenez, J. L., Adachi, K., Buseck, P. R., Hall, S. R., and Shetter, R.: Emissions from biomass burning in the Yucatan, Atmos. Chem. Phys., 9, 5785-5812, https://doi.org/10.5194/acp-9-5785-2009, 2009.

Yokelson, R. J., Goode, J. G., Ward, D. E., Susott, R. A., Babbitt, R. E., Wade, D. D., Bertschi, I., Griffith, D. W. T., and Hao, W. M.: Emissions of formaldehyde, acetic acid, methanol, and other trace gases from biomass fires in North Carolina measured by airborne Fourier transform infrared spectroscopy, J. Geophys. Res.-Atmos, 104, 30109-30125, https://doi.org/10.1029/1999JD900817, 1999.

Yokelson, R. J., Griffith, D. W. T., and Ward, D. E.: Open-path Fourier transform infrared studies of large-scale laboratory biomass fires, J. Geophys. Res.-Atmos, 101, 21067-21080, https://doi.org/10.1029/96JD01800, 1996.

Yokelson, R. J., Karl, T., Artaxo, P., Blake, D. R., Christian, T. J., Griffith, D. W. T., Guenther, A., and Hao, W. M.: The tropical forest and fire emissions experiment: Overview and airborne fire emission factor measurements, Atmos. Chem. Phys., 7, 5175-5196, https://doi.org/10.5194/acp-7-5175-2007, 2007.

Yokelson, R. J., Susott, R., Ward, D. E., Reardon, J., and Griffith, D. W. T.: Emissions from smoldering combustion of biomass measured by open-path Fourier transform infrared spectroscopy, J. Geophys. Res.-Atmos, 102, 18865-18877, https://doi.org/10.1029/97JD00852, 1997.

Yu, S.: Role of organic acids (formic, acetic, pyruvic and oxalic) in the formation of cloud condensation nuclei (CCN): a review, Atmos. Res., 53, 185-217, https://doi.org/10.1016/S0169-8095(00)00037-5, 2000.

Yu, P., Toon, O. B., Bardeen, C. G., Zhu, Y., Rosenlof, K. H., Portmann, R. W., Thornberry, T. D., Gao, R.-S., Davis, S. M., Wolf, E. T., Gouw, J. d., Peterson, D. A., Fromm, M. D., and Robock, A.: Black carbon lofts wildfire smoke high into the stratosphere to form a persistent plume, Science, 365, 587-590, https://doi.org/10.1126/science.aax1748, 2019.

Zhang, R., Suh, I., Zhao, J., Zhang, D., Fortner, E. C., Tie, X., Molina, L. T., and Molina, M. J.: Atmospheric new particle formation enhanced by organic acids, Science, 304, 1487-1490, https://doi.org/10.1126/science.1095139, 2004.

https://doi.org/10.5194/acp-2022-245
Preprint. Discussion started: 14 April 2022

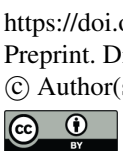

Atmospheric Chemistry and Physics Discussions

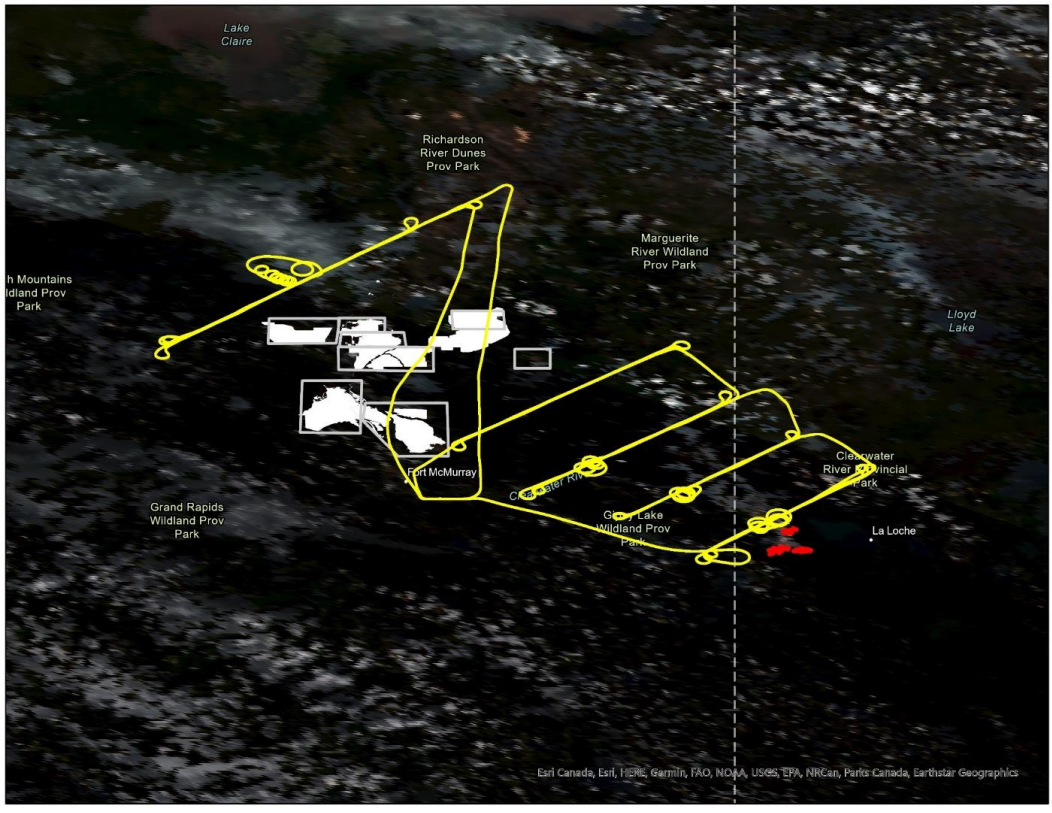

Figure 1. Corrected reflectance satellite image from the VIIRS spectroradiometer on the Suomi NPP and NOAA-20 satellites taken on June 25, 2018. The fire hot spots for the wildfire of interest are indicated by the red dots. Flight tracks were flow at Lagrangian distances downwind of the wildfire. Multiple transects at varying altitudes perpendicular to the plume direction formed virtual screens. Plume direction of travel is indicated by the large arrow. The location of the Alberta oil sands mining facilities are shown in white.

https://doi.org/10.5194/acp-2022-245
Preprint. Discussion started: 14 April 2022

Atmospheric Chemistry and Physics Discussions

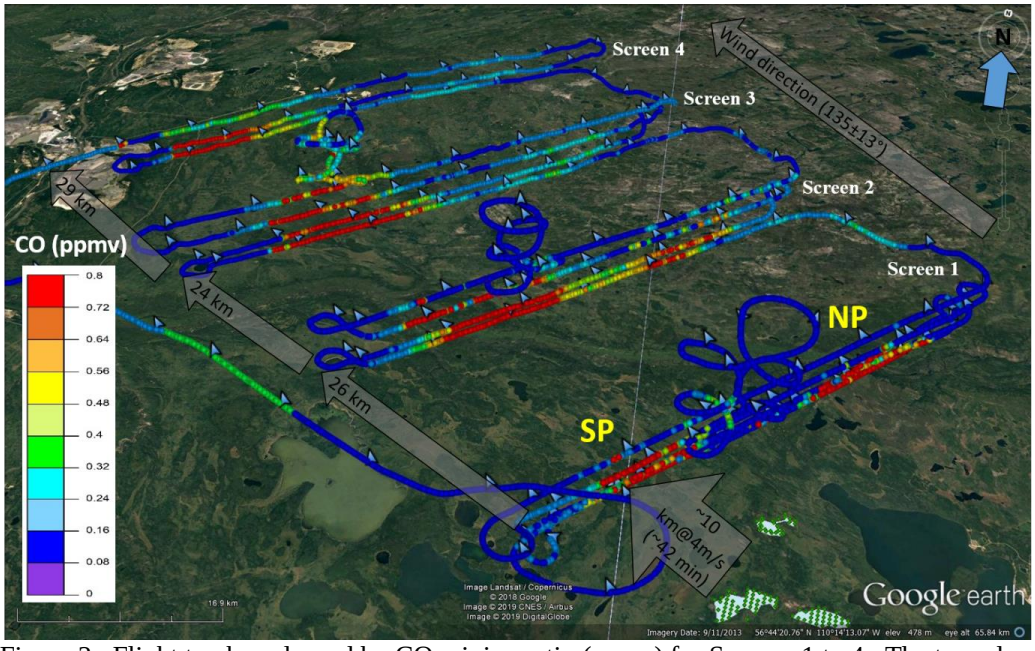

Figure 2. Flight tracks coloured by CO mixing ratio (ppmv) for Screens 1 to 4. The two plumes are identified as south plume (SP) and north plume (NP). The fire perimeter surrounding the detected MODIS-derived 'hot spots' on June 25, 2018 is shown in the green hatched area. The source of the NP is expected to be the same hot spots as the SP but ~ 30 min older; see SI Sect. 2.2. The small blue arrows along the flight tracks indicate the aircraft measured wind direction with the average wind direction depicted with the large gray arrow. Distances between screens are shown in the grey arrows.

https://doi.org/10.5194/acp-2022-245
Preprint. Discussion started: 14 April 2022

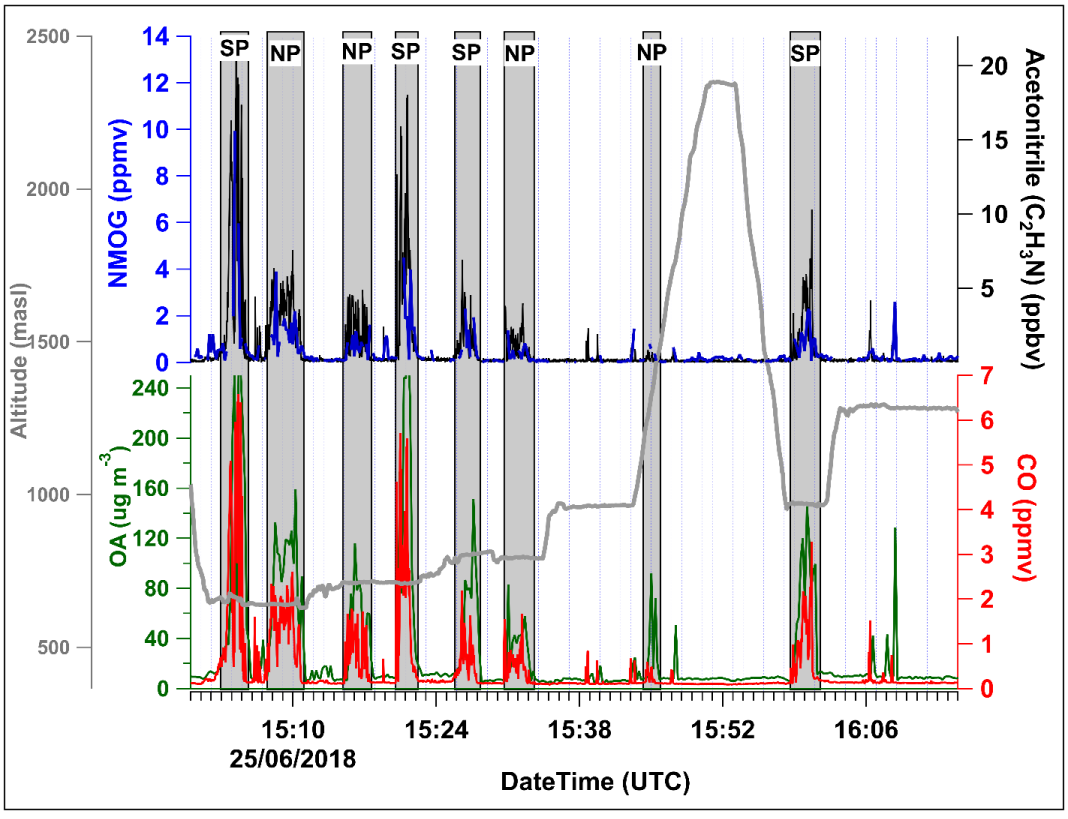

Figure 3. Time series of NMOGs, acetonitrile (C_2H_3N) and CO mixing ratios, as well as OA concentrations and altitude for Screen 1. The in-plume portions are indicated by the vertical grey bars. The aircraft flew back and forth across the plumes at increasing altitudes to complete five transects; a transect represents one pass across the SP and NP at the same altitude.

https://doi.org/10.5194/acp-2022-245
Preprint. Discussion started: 14 April 2022

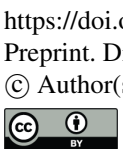

Atmospheric Chemistry and Physics Discussions

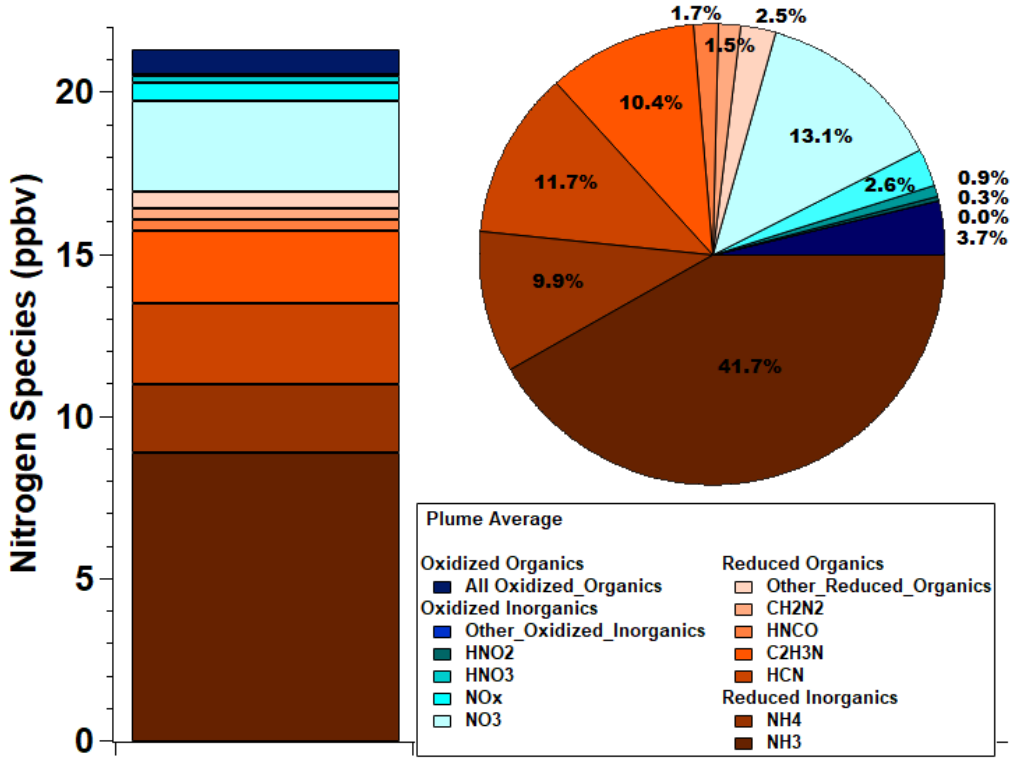

Figure 4. Background-subtracted average Screen 1 in-plume mixing ratios of measured gas- and particle-phase N-containing species (N_r) and their fractional contribution to the total summed N_r species. The N_r species are grouped into categories of reduced inorganics, reduced organics, oxidized inorganics and oxidized organics with reduced species in shades of red and oxidized species in shades of blue.

https://doi.org/10.5194/acp-2022-245
Preprint. Discussion started: 14 April 2022

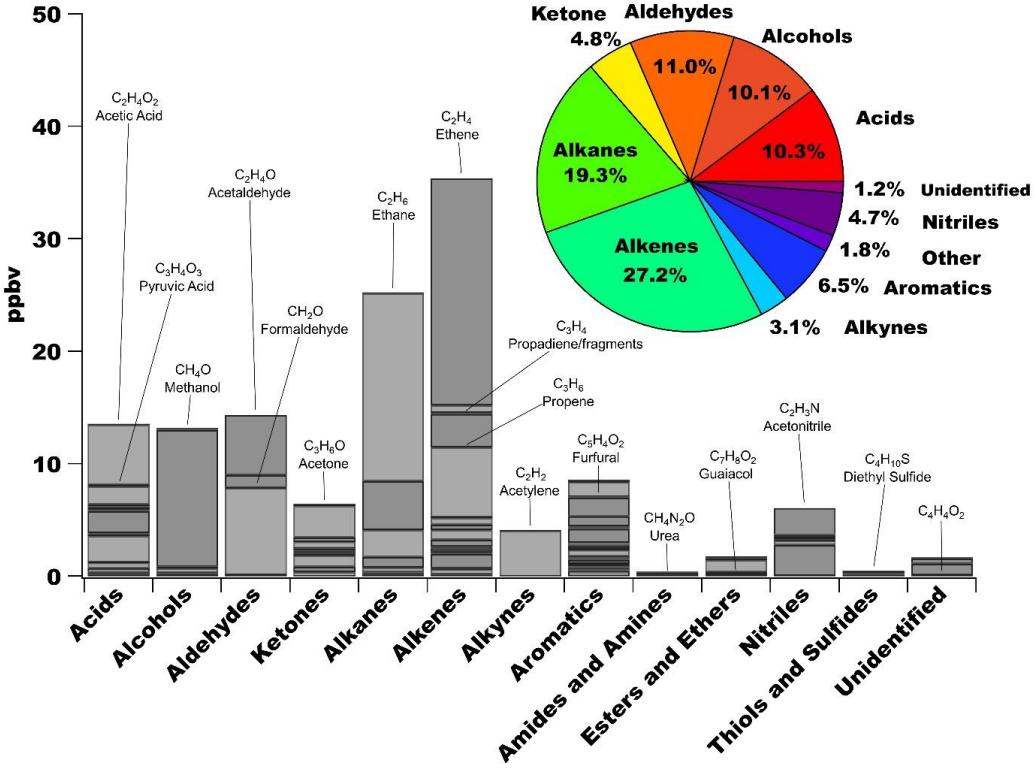

Figure 5. Background-subtracted average mixing ratios of individually measured NMOGs shown for thirteen chemical classes. In some cases, compounds are double- (or triple-) counted if they can be identified in more than one category. For example, phenol is an alcohol + an aromatic; guaiacol is an alcohol + an ether + an aromatic. In the pie chart, the *Other* category includes amides, amines, ethers, thiols and sulfides. The unidentified category contains molecular formulas detected but the compound(s) could not be identified.

https://doi.org/10.5194/acp-2022-245
Preprint. Discussion started: 14 April 2022

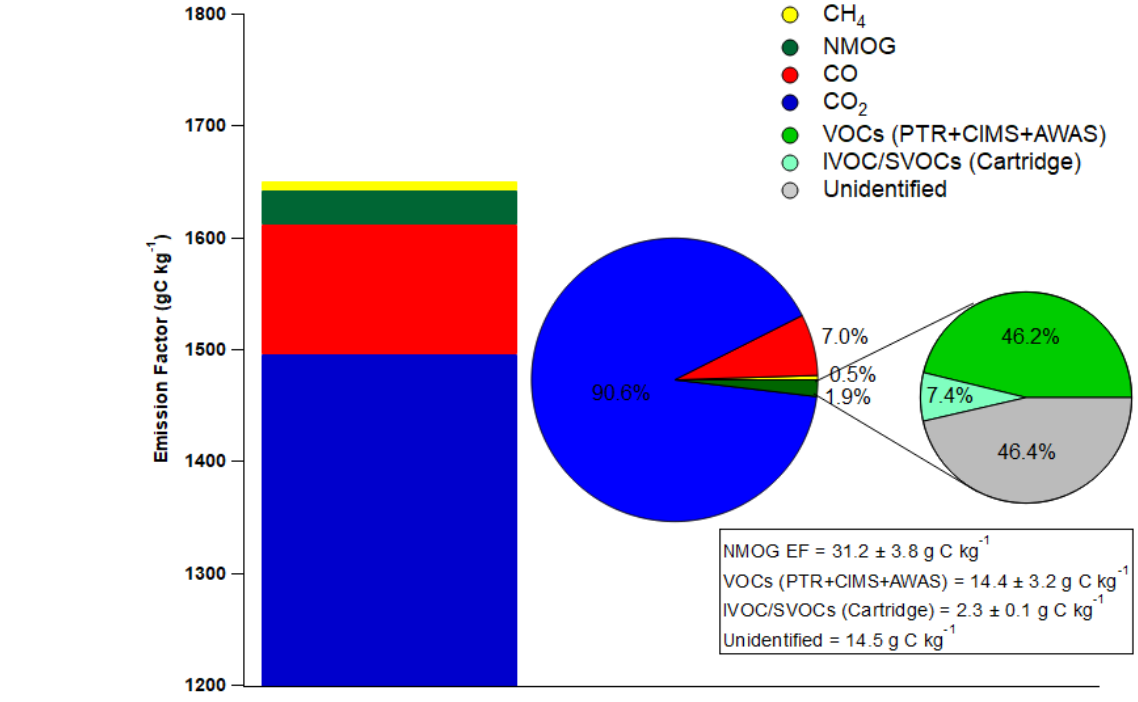

Figure 6. Total carbon (TC) partitioning based on EFs (carbon fraction). The bar chart shows the stacked EFs for carbon-containing compounds with the middle pie chart showing their percent contributions to the TC. The pie chart on the right show the percent breakdown of the measured NMOGs with the remaining unidentified portion in terms of g C kg^{-1}. Note that all the EFs shown in Table A1 were converted to g C kg^{-1}.

https://doi.org/10.5194/acp-2022-245
Preprint. Discussion started: 14 April 2022

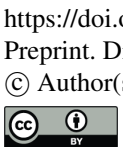

Atmospheric Chemistry and Physics Discussions

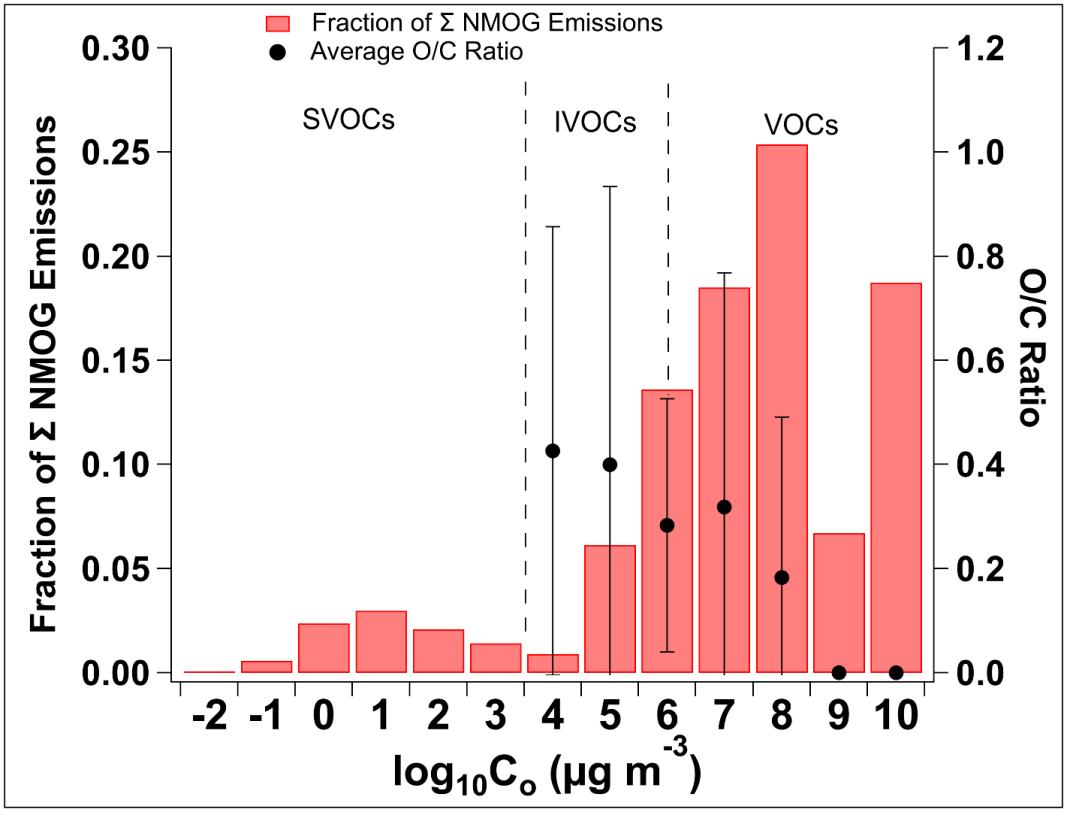

Figure 7. Fraction of total NMOG emissions in each volatility bin, as well as the bin-averaged O/C ratio spanning VOCs, IVOCs and SVOCs. Data is included from PTRMS, CIMS, AWAS and cartridge measurements. The O/C ratio is derived for only the PTRMS, CIMS and AWAS measurements and the errors bars indicate the standard deviation of the average O/C ratio.

https://doi.org/10.5194/acp-2022-245
Preprint. Discussion started: 14 April 2022

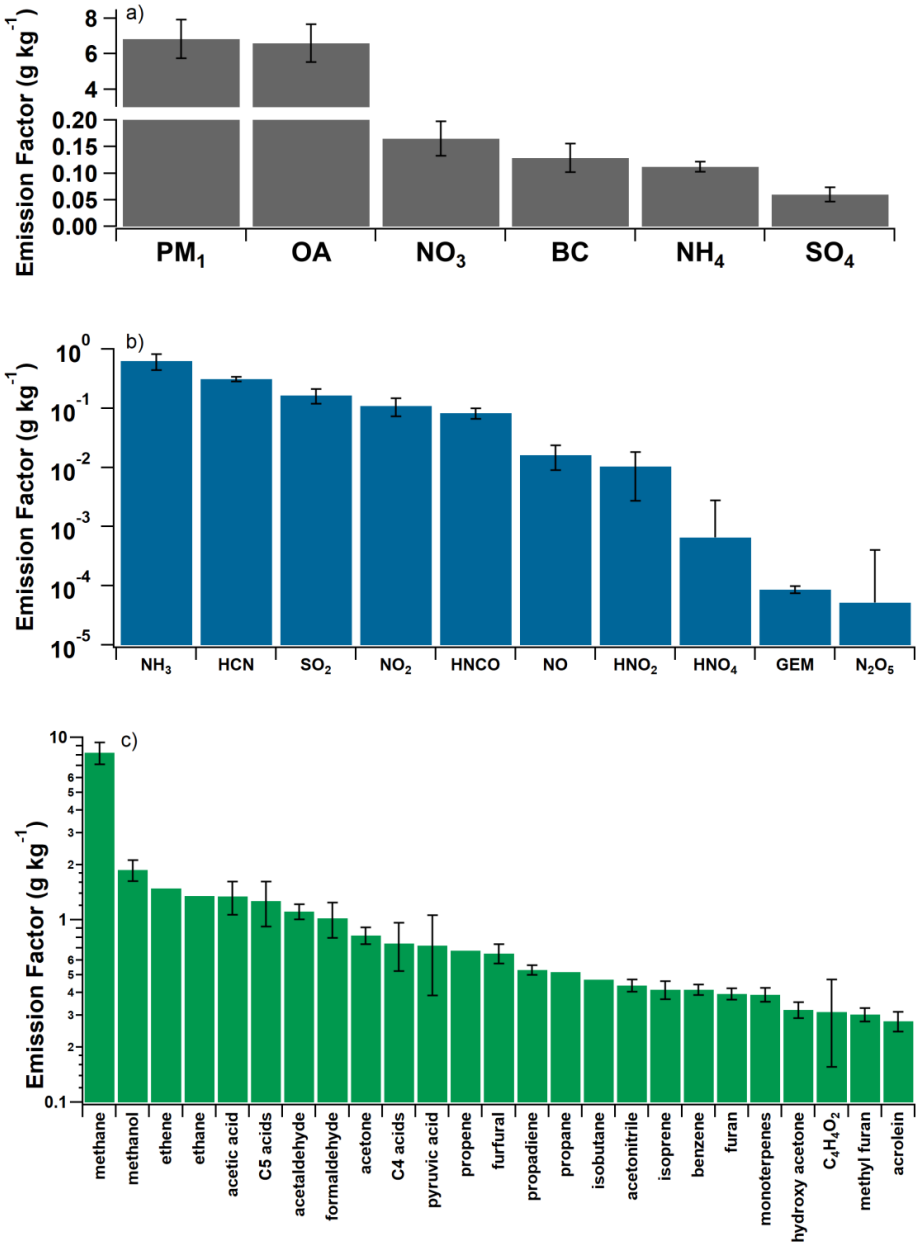

Figure 8. Average emission factors (g kg^{-1}) of a) particle species; b) inorganic gas-phase species, and c) the top 25 measured gas-phase organic species. C5 acids = C5 oxo-carboxylic acids; C4 acids = C4 oxo-carboxylic acids; propadiene = fragments/propadiene; hydroxy acetone = hydroxy acetone/ ethyl formate. Organic species measurements are from the PTRMS, CIMS and AWAS.

https://doi.org/10.5194/acp-2022-245
Preprint. Discussion started: 14 April 2022

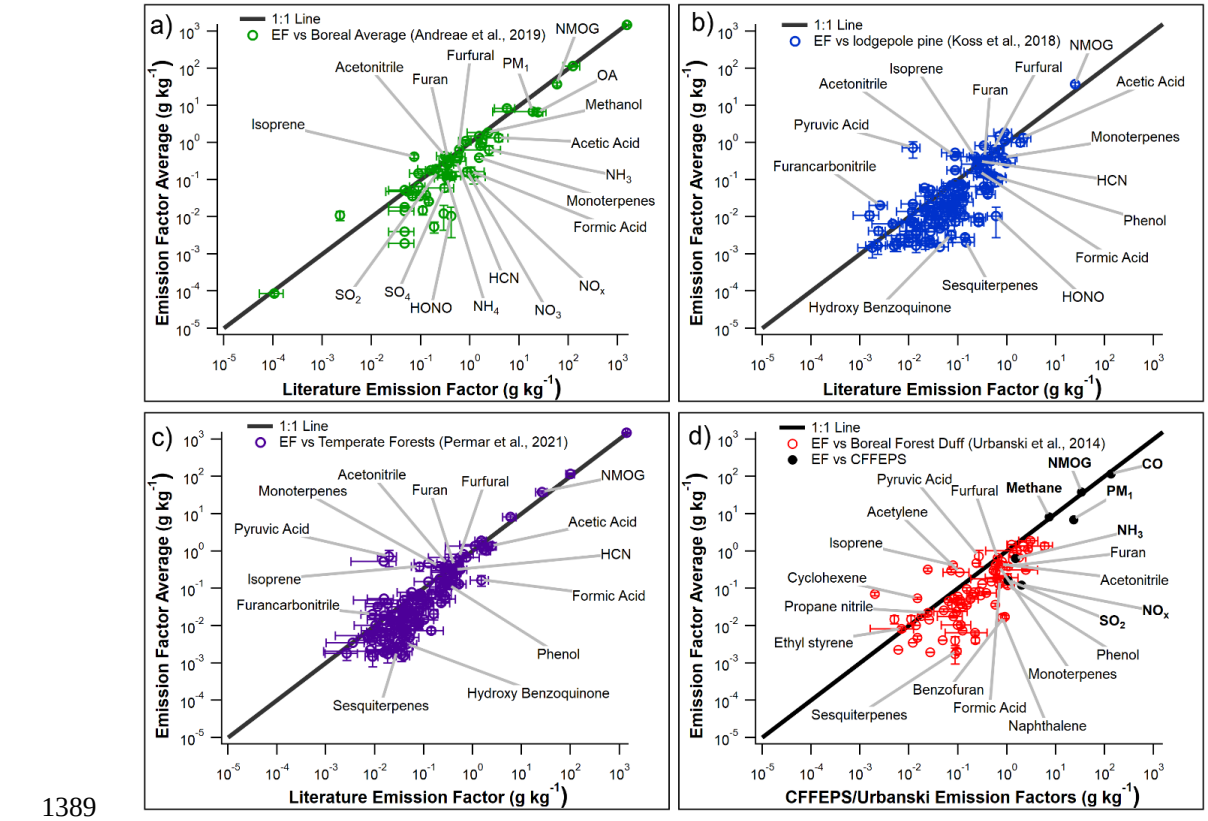

Figure 9. Comparison of averaged emission factors with a) boreal forest field-based measurements (Andreae, 2019; Akagi et al., 2011; Liu et al., 2017), b) laboratory-based measurements of lodgepole pine (Koss et al., 2018), c) temperate forest field-based measurements (Permar et al., 2021), and d) those used in CFFEPS (Urbanski et al., 2014). See Table S8 for compound comparisons that don't have exact matches.

https://doi.org/10.5194/acp-2022-245
Preprint. Discussion started: 14 April 2022

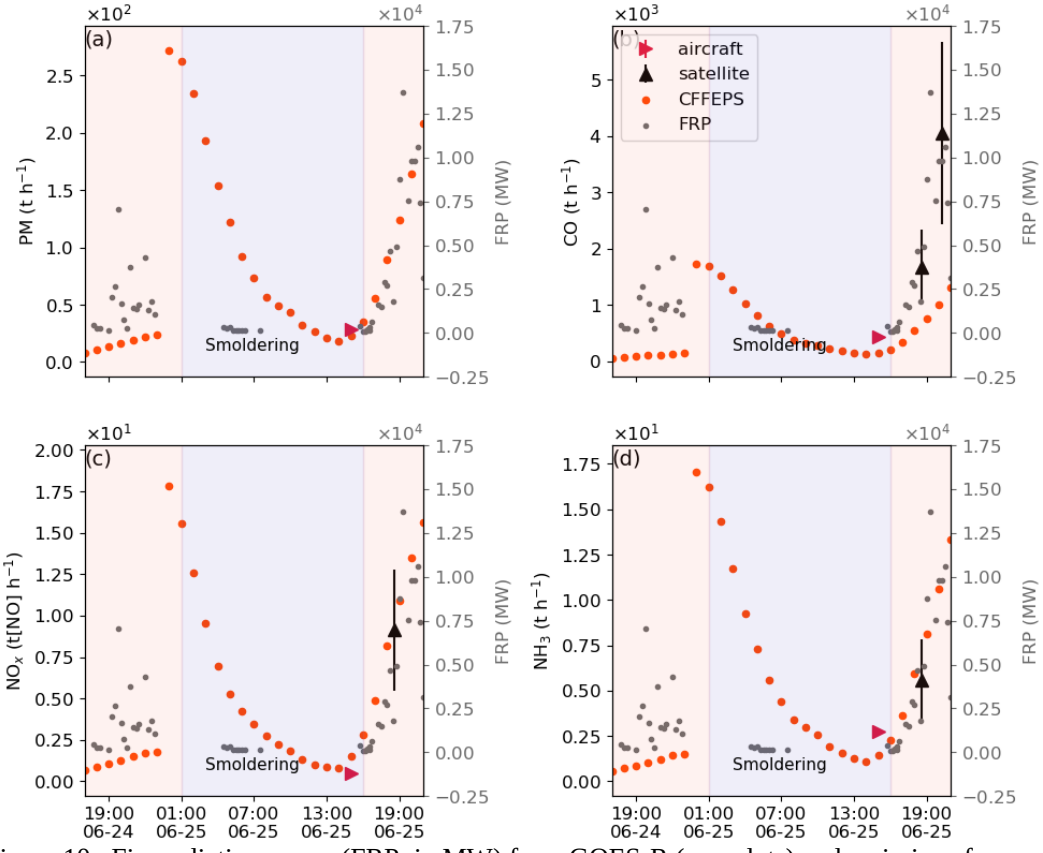

Figure 10. Fire radiative power (FRP; in MW) from GOES-R (grey dots) and emissions from the CFFEPS model (orange dots) from 2018-06-24 17:00 UTC to 2018-06-25 21:00 UTC. Aircraft-derived emission rates are shown for a) PM_1, b) CO, c) NO_x (as NO) and d) NH_3 (in t h^{-1}; red arrow) at 15:00 UTC when the aircraft flew closest to the fire. The corresponding TROPOMI satellite-derived emission rates are also shown (in t h^{-1}; black arrows). Note, the aircraft flight time occurred when the fire intensity reflected a surface, smoldering fire and the satellite overpass time took place when the fire had transitioned to a crown (flaming) fire. The smoldering and flaming time periods are coloured in blue and pink, respectively.

https://doi.org/10.5194/acp-2022-245
Preprint. Discussion started: 14 April 2022

Atmospheric Chemistry and Physics Discussions

Table A1

Table S7. Summary of emission factors (g kg^{-1}) (EF) and emission ratios (ppb ppm^{-1}; particulates in µg m^{-3} ppm^{-1} and TGM in ng m^{-3} ppm^{-1}) (ER) for the SP, NP, and the EF average of the two plumes, grouped by particulate species, and inorganic and organic gas-phase species (sorted by increasing molecular weight). PM_1 is the sum of all the particulate species. The CE was 0.84±0.04 and 0.82±0.01 for the SP and NP, respectively. For comparison, EFs are also included from previously published literature: Andreae (2019)[1], Liu et al. (2017)[a]; Akagi et al. (2011)[b]; and Simpson et al. (2011)[c]), Koss et al. (2018)[2] and Permar et al. (2021)[3]. See Table S8 for compounds that did not have exact matches for comparison to literature values. For species measured in mass concentration units, Eq. 2 was modified by converting TC to mass concentrations using the measured temperature and pressure, and removing the molar mass ratio term. * Indicates that the compound was 'calculated' (SI Sect 2.1.1) while the remaining compounds were calibrated. **Estimated, see text in Sect. 3.4.3. ***Uncertainty reflects the standard deviation of the calibration.

Molecular Weight	Compound	Compound Name	Instru-ment	Average EF (g kg^{-1})	NP EF (g kg^{-1})	SP EF (g kg^{-1})	Literature EF (g kg^{-1})	NP ER	SP ER
Particulate									
	PM_1	particulate matter (<1µm)	AMS	6.8±1.1	7.1±0.48	6.6±2.1	18.8±15.9[1]	59±1.5	65±15
	BC	black carbon	SP2	0.13±0.027	0.11±0.0098	0.14±0.052	0.43±0.21[1] 0.39±0.17[3]	0.55±0.026	0.58±0.32
	NH_4	p-ammonium	AMS	0.11±0.097	0.11±0.0069	0.12±0.018	0.34±0.15[1, a]	1.1±0.066	1.9±0.43
	NO_3	p-nitrate	AMS	0.17±0.032	0.14±0.013	0.19±0.064	0.87±0.13[1, a]	0.9±0.02	1.2±0.028
	SO_4	p-sulphate	AMS	0.06±0.013	0.066±0.003	0.055±0.026	0.30±0.16[1, a]	0.035±0.00077	0.054±0.015
	OA	p-total organics	AMS	6.6±1.1	6.9±0.33	6.3±2.1	24.3±0.21[1, a]	58±0.6	62±15
Gas Inorganic									
17.031	NH_3	ammonia	LGR	0.63±0.19	0.45±0.071	0.82±0.37	2.5±1.8[1] 0.68±0.19[2]	5.8±0.9	13±4.7
27.026	HCN	hydrogen cyanide	CIMS	0.31±0.028	0.34±0.026	0.29±0.049	0.53±0.30[1] 0.28±0.06[2] 0.43±0.17[3]	2.8±0.19	2.9±0.34
28.01	CO	carbon monoxide	Picarro	115.7±7.5	127±5.6	104.1±14.0	120±47[1] 99±20[3]	110±67	130±100
30.006	NO	nitric oxide	TECOs	0.016±0.0072	0.017±0.0081	0.016±0.012	0.29[1]	0.12±0.068	0.14±0.09
43.025	HNCO	isocyanic acid	CIMS	0.083±0.017	0.091±0.018	0.076±0.03	0.57±0.24[2] 0.16±0.036[3]	0.46±0.074	0.47±1.8
43.025	HNCO	isocyanic acid*	PTRMS	0.021±0.0065	0.015±0.0025	0.026±0.013	0.57±0.24[2]	0.078±0.011	0.16±0.066
44.009	CO_2	carbon dioxide	Picarro	1496.3±35.8	1481.7±18.4	1510.9±69.2	1500±140[1] 1400±61[3]	7400±360	9400±340
46.005	NO_2	nitrogen dioxide	TECOs	0.11±0.037	0.076±0.0077	0.15±0.074		0.37±0.052	0.83±0.37
46.005	NO_x	sum ($NO+NO_2$)	TECOs	0.12±0.045	0.072±0.037	0.17±0.083	1.2±0.86[1]	0.34±0.17	0.97±1.2

https://doi.org/10.5194/acp-2022-245
Preprint. Discussion started: 14 April 2022

Atmospheric Chemistry and Physics Discussions

47.013	HNO_2	nitrous acid	CIMS	0.01±0.0077	0.00048±0.0018	0.02±0.015	0.41[1] 0.6±0.20[2]		0.11±0.077
64.064	SO_2	sulphur dioxide	TECOs	0.17±0.046	0.074±0.032	0.26±0.085	0.22±0.31[1]	0.26±0.13	1.1±0.29
79.011	HNO_4	peroxynitric acid	CIMS	0.00066±0.0021	0.00047±0.0042	0.00085±0.00059		0.00089±0.012	0.0028±0.0019
108.009	N_2O_5	dinitrogen pentoxide	CIMS	5.2E-5±0.00035	0.00025±0.00051	-0.00015±0.005		0.00048±0.001	-0.0003±0.0012
200.59	GEM	gaseous elemental mercury	Tekran	8.7E-5±1.2E-5	8.2E-5±1.4E-5	9.2E-5±1.9E-5	0.00023±0.0003[1]	0.00068±0.00012	0.00091±0.0001
Gas Organic									
	ΣNMOG	non methane organic gases	PTRMS+ClMS+AWAS+ cartridges	25.8±3.2	26.2±2.1	25.4±5.8			
	Estimate $NMOG_{Ty}$	non methane organic gases	PTRMS+ClMS+AWAS+ cartridges	37.8 to 39.9**			58.7[1, b] 25.0[2] 26.1[3]		
	$NMOG_T$ (g **C**/kg)	Carbon fraction of non methane organic gases	Picarro	31.2±3.8	36.8±5.1	25.5±5.6		680±120	580±150
16.043	CH_4	methane	Picarro	8.3±1.1	7.8±0.4	8.7±2.2	5.5±2.5[1] 5.9±1.8[3]	110±1.3	150±30
26.038	C_2H_2	acetylene	AWAS	0.27	0.20	0.34	0.31±0.17[3]	2.2	4
27.046	C_2H_3	fragment vinyl/ethane*	PTRMS	0.012±0.0017	0.012±0.0011	0.012±0.0032		0.096±0.013	0.12±0.017
28.054	C_2H_4	ethene	AWAS	1.49	1.29	1.69	1.5±0.66[1] 0.71±0.31[2] 1.5±1[3]	12.94	18.31
30.026	CH_2O	formaldehyde	PTRMS	1.0±0.22	1.1±0.14	0.93±0.43	1.8±0.4[1] 1.9±0.67[2] 1.9±0.43[3]	8.1±0.68	8.9±3.3
30.07	C_2H_6	ethane*	AWAS	1.3	1.3	1.4	1.1±0.84[3]	12	14
32.042	CH_4O	methanol	PTRMS	1.9±0.25	2.2±0.21	1.6±0.45	2.3±1.4[1] 0.9±0.35[2] 1.5±0.39[3]	15±0.85	13±3.9
40.065	C_3H_4	fragments/propadiene*	PTRMS	0.53±0.032	0.64±0.037	0.42±0.051	0.06±0.03[1] 0.088±0.041[2]	3.5±0.062	2.8±0.21
41.053	C_2H_3N	acetonitrile	PTRMS	0.44±0.034	0.48±0.028	0.4±0.062	0.31±0.099[1] 0.086±0.028[2] 0.31±0.15[3]	2.6±0.066	2.6±0.1
42.037	C_2H_2O	acetic acid fragment*	PTRMS	1.45±0.17	1.46±0.12	1.43±0.32		7.67±0.32	9.05±1.08
42.041	CH_2N_2	cyanamide*	PTRMS	0.064±0.0087	0.067±0.00038	0.061±0.017		1.4±0.017	1.3±0.074
42.081	C_3H_6	propene	AWAS	0.68	0.62	0.73	0.74±0.62[3]	4.2	5.2
44.053	C_2H_4O	acetaldehyde	PTRMS	1.1±0.11	1.2±0.074	1.0±0.2	0.81±0.23[1] 0.92±0.32[2] 1.7±0.43[3]	6.3±0.42	6.3±0.48
44.097	C_3H_8	propane	AWAS	0.52	0.53	0.50	0.46±0.18[3]	3.4	3.4
46.025	CH_2O_2	formic acid	CIMS	0.17±0.053	0.17±0.032	0.17±0.10	1±0.89[1] 0.28±0.14[2] 1.5±0.60[3]	1.2±0.093	0.56±0.82

https://doi.org/10.5194/acp-2022-245
Preprint. Discussion started: 14 April 2022

Atmospheric Chemistry and Physics Discussions

48.103	CH_4S	methanethiol *	PTRMS	0.014±0.0016	0.015±0.0021	0.013±0.0025	0.011±0.006[2]	0.068±0.0091	0.073±0.0081
50.057	CH_6O_2	methanol hydrate*	PTRMS	0.028±0.0057	0.034±0.0023	0.022±0.011		0.15±0.0077	0.12±0.065
52.076	C_4H_4	buten-yne/fragments*	PTRMS	0.018±0.0016	0.02±0.0011	0.016±0.0031	0.057±0.032[2] 0.052±0.018[3]	0.086±0.0043	0.081±0.0069
53.064	C_3H_3N	acrylonitrile*	PTRMS	0.036±0.0029	0.04±0.0024	0.032±0.0052	0.025±0.012[2] 0.044±0.015[3]	0.17±0.0032	0.16±0.0054
54.048	C_3H_2O	propynal*	PTRMS	0.0087±0.0034	0.0045±0.0032	0.013±0.006	0.034±0.014[2] 0.037±0.015[3]	0.018±0.013	0.062±0.024
54.092	C_4H_6	butadiene/fragments*	PTRMS	0.15±0.016	0.15±0.004	0.15±0.031	0.089±0.03[1] 0.34±0.18[2] 0.27±0.096[3]	0.62±0.014	0.73±0.067
54.092	C_4H_6	1,3-butadiene	AWAS	0.065	0.055	0.075	0.089±0.03[1] 0.34±0.18[2] 0.27±0.096[3]	0.29	0.41
55.08	C_3H_5N	propane nitrile*	PTRMS	0.022±0.0017	0.025±0.0017	0.019±0.003	0.012±0.0051[2] 0.037±0.018[3]	0.1±0.0038	0.094±0.042
56.064	C_3H_4O	acrolein	PTRMS	0.28±0.035	0.29±0.025	0.26±0.065	0.335[1] 0.97±0.5[2] 0.4±0.18[3]	0.82±0.04	0.83±0.038
56.108	C_4H_8	cis-2-butene	AWAS	0.011	0.0061	0.015		0.03	0.078
56.108	C_4H_8	isobutene	AWAS	0.084	0.082	0.086		0.41	0.45
56.108	C_4H_8	t-2,butene	AWAS	0.0074	0.0026	0.012		0.013	0.063
56.108	C_4H_8	1,butene	AWAS	0.13	0.12	0.14		0.6	0.74
57.052	C_2H_3NO	hydroxy acetonitrile	CIMS	0.0035±0.00059	0.0025±0.0002	0.0044±0.0012	0.014±0.0048[2] 0.033±0.0087[3]	0.026±0.0059	0.024±0.0047
57.052	C_2H_3NO	methyl isocyanate*	PTRMS	0.006±0.012	0.0068±0.0017	0.0052±0.0015	0.014±0.0048[2] 0.033±0.0087[3]	0.026±0.0059	0.024±0.0047
57.096	C_3H_7N	propene amine*	PTRMS	0.0017±0.00073	0.0016±0.00086	0.0019±0.0012	0.0023±0.00099[2] 0.018±0.0082[3]	0.0061±0.0033	0.0086±0.0053
58.08	C_3H_6O	acetone	PTRMS	0.82±0.088	0.99±0.13	0.65±0.12	1.6±1.6[1] 0.34±0.12[2] 0.65±0.38[3]	0.065±0.014	0.072±0.042
58.124	C_4H_{10}	isobutane	AWAS	0.47	0.52	0.42	0.12±0.061[3]	2.6	2.2
58.124	C_4H_{10}	n-butane*	AWAS	0.15	0.16	0.14	0.12±0.061[3]	0.79	0.73
59.068	C_2H_5NO	acetamide*	PTRMS	0.0016±0.0021	0.0054±0.0038	-0.0023±0.0017	0.043±0.021[2] 0.04±0.012[3]	0.02±0.014	-0.01±0.0068
60.052	$C_2H_4O_2$	acetic acid	CIMS	1.3±0.28	1.1±0.19	1.6±0.53	3.8±2.1[1] 2.2±0.89[2] 2.4±0.61[3]	7.4±0.37	8.9±1
60.056	CH_4N_2O	urea*	PTRMS	0.078±0.012	0.079±0.015	0.076±0.019		0.29±0.044	0.34±0.048
60.096	C_3H_8O	propanol*	PTRMS	0.0054±0.0017	0.0061±0.0024	0.0046±0.0025	0.0074±0.0058[3]	0.022±0.0082	0.02±0.0097
61.04	CH_3NO_2	nitromethane *	PTRMS	0.011±0.0021	0.01±0.0011	0.011±0.004	0.074±0.03[2] 0.078±0.0085[3]	0.036±0.0049	0.048±0.013
62.068	$C_2H_6O_2$	ethylene glycol*	PTRMS	0.0038±0.00047	0.004±0.00041	0.0036±0.00086		0.014±0.0084	0.015±0.0036
62.13	C_2H_6S	dimethyl sulfide	PTRMS	0.011±0.0031	0.016±0.0061	0.0067±0.0014	0.0047[1, a] 0.0016±0.00084[2] 0.08±0.083[3]	0.017±0.004	0.029±0.065

https://doi.org/10.5194/acp-2022-245
Preprint. Discussion started: 14 April 2022

Atmospheric Chemistry and Physics Discussions

64.04	CH_4O_3	methanetriol *	PTRMS	0.0011±0.0025	0.0036±0.00059	-0.0013±0.005		0.013±0.0024	-0.0049±0.02
64.087	C_5H_4	*	PTRMS	0.003±0.00091	0.0042±0.0017	0.0017±0.00076		0.014±0.0052	0.0074±0.003
66.103	C_5H_6	cyclopentadiene*	PTRMS	0.032±0.0031	0.041±0.0047	0.023±0.0042	0.011±0.0049[3]	0.14±0.012	0.096±0.014
67.091	C_4H_5N	pyrrole*	PTRMS	0.026±0.0022	0.027±0.00062	0.025±0.0043	0.054±0.029[2] 0.039±0.021[3]	0.09±0.0051	0.098±0.0067
68.075	C_4H_4O	furan*	PTRMS	0.39±0.028	0.43±0.02	0.35±0.052	0.36±0.44[1] 0.36±0.11[2] 0.43±0.19[3]	1.4±0.049	1.4±0.076
68.119	C_5H_8	isoprene	PTRMS	0.41±0.10	0.64±0.078	0.19±0.06	0.074[1] 0.22±0.11[2] 0.082±0.095[3]	2.1±0.22	0.47±0.61
69.083	C_4H_5O	*	PTRMS	0.0043±0.00039	0.0047±0.00016	0.0038±0.00077		0.015±0.0012	0.015±0.0019
69.107	C_4H_7N	butane nitrile*	PTRMS	0.0077±0.00064	0.0088±0.00061	0.0065±0.0011	0.011±0.0048[2] 0.02±0.01[3]	0.028±0.00085	0.025±0.0018
70.091	C_4H_6O	methyl vinyl ketone, methacrolein, crotonaldehyde	PTRMS	0.19±0.055	0.2±0.0039	0.18±0.11	0.11±0.12[1] 0.34±0.15[2] 0.39±0.15[3]	0.66±0.013	0.68±0.37
70.135	C_5H_{10}	pentene/fragments*	PTRMS	0.018±0.0017	0.019±0.0022	0.018±0.0025	0.046±0.025[1] 0.028±0.01[2] 0.015±0.0084[3]	0.059±0.009	0.069±0.0053
70.135	C_5H_{10}	c-2-pentene	AWAS	0.004	0.0033	0.0048	0.046±0.025[1] 0.028±0.01[2] 0.015±0.0084[3]	0.013	0.021
70.135	C_5H_{10}	cyclopentane	AWAS	0.0035	0.0038	0.0031	0.0035±0.0025[3]	0.016	0.014
70.135	C_5H_{10}	1-pentene	AWAS	0.052	0.053	0.052	0.046±0.025[1] 0.028±0.01[2] 0.015±0.0084[3]	0.21	0.22
70.135	C_5H_{10}	2-methyl,1-butene	AWAS	0.014	0.014	0.015	0.046±0.025[1] 0.028±0.01[2] 0.015±0.0084[3]	0.056	0.062
70.135	C_5H_{10}	2-methyl,2-butene	AWAS	0.0019	0.0017	0.0022	0.046±0.025[1] 0.028±0.01[2] 0.015±0.0084[3]	0.0068	0.0095
72.063	$C_3H_4O_2$	acrylic acid	CIMS	0.096±0.0098	0.13±0.0091	0.062±0.017	0.22±0.082[3]	0.25±0.0095	0.35±0.087
72.107	C_4H_8O	MEK + butanal + 2-methylpropanal	PTRMS	0.18±0.015	0.22±0.012	0.14±0.027	0.16±0.036[1] 0.087±0.028[2] 0.21±0.063[3]	0.67±0.01	0.54±0.063
72.151	C_5H_{12}	n-pentane	AWAS	0.078	0.086	0.07	0.057±0.028[3]	0.34	0.29
72.151	C_5H_{12}	2-methylbutane	AWAS	0.022	0.024	0.021	0.057±0.028[3]	0.097	0.086
73.095	C_3H_7NO	dimethylformamide*	PTRMS	0.001±0.0006	0.0018±0.00052	0.00024±0.0011		0.0053±0.0014	0.0011±0.0038
74.079	$C_3H_6O_2$	propionic acid	CIMS	0.13±0.04	0.12±0.0042	0.14±0.08		1±0.041	1.1±0.096
74.079	$C_3H_6O_2$	hydroxy acetone/ethyl formate*	PTRMS	0.32±0.033	0.35±0.025	0.3±0.06	0.49±0.19[2] 0.57±0.2[3]	1±0.041	1.1±0.096

https://doi.org/10.5194/acp-2022-245
Preprint. Discussion started: 14 April 2022

Atmospheric Chemistry and Physics Discussions

78.114	C_6H_6	benzene	PTRMS	0.41±0.027	0.47±0.021	0.36±0.05	0.57±0.21[1] 0.42±0.25[2] 0.5±0.14[3]	1.3±0.0016	1.2±0.046
80.086	C_5H_4O	cyclopentadienone/isomers*	PTRMS	0.011±0.0014	0.0093±0.00043	0.012±0.0028	0.13±0.075[2] 0.027±0.017[3]	0.026±0.0017	0.04±0.0068
80.13	C_6H_8	cyclohexadiene/monoterpene fragment*	PTRMS	0.14±0.01	0.17±0.011	0.1±0.018		0.48±0.037	0.34±0.06
81.094	C_5H_5O	*	PTRMS	0.0039±0.00084	0.004±0.00032	0.0037±0.0016		0.011±0.00039	0.012±0.0045
81.118	C_5H_7N	pentene nitriles/methyl pyrrole*	PTRMS	0.0047±0.00051	0.005±0.00012	0.0044±0.001	0.02±0.011[3]	0.014±0.00029	0.015±0.002
82.102	C_5H_6O	methyl furan*	PTRMS	0.3±0.026	0.31±0.011	0.29±0.05	0.32±0.11[2] 0.28±0.13[3]	0.84±0.047	0.96±0.041
82.146	C_6H_{10}	cyclohexene*	PTRMS	0.054±0.0035	0.075±0.0029	0.033±0.0064		0.2±0.012	0.11±0.013
83.09	C_4H_5NO	methyloxazole*	PTRMS	0.003±0.00052	0.0039±0.001	0.002±0.00018		0.01±0.0023	0.0066±0.00067
83.134	C_5H_9N	pentanenitriles*	PTRMS	0.016±0.00096	0.019±0.00046	0.013±0.0019	0.021±0.011[3]	0.049±0.0011	0.042±0.0048
84.074	$C_4H_4O_2$		CIMS	0.31±0.16	0.1±0.092	0.52±0.3		0.42±0.026	0.48±0.072
84.074	$C_4H_4O_2$	furanone*	PTRMS	0.16±0.02	0.16±0.017	0.15±0.036	0.4±0.15[2] 0.32±0.11[3]	0.42±0.026	0.48±0.072
84.118	C_5H_8O	cyclopentanone/isomers*	PTRMS	0.069±0.0056	0.073±0.004	0.065±0.011	0.12±0.04[2] 0.087±0.038[3]	0.19±0.012	0.21±0.0077
84.162	C_6H_{12}	hexene*	PTRMS	0.015±0.0036	0.02±0.0033	0.0098±0.0064	0.11[1]	0.052±0.0064	0.031±0.017
84.162	C_6H_{12}	cis-2-hexene	AWAS	0.0020	0.0021	0.0020		0.0069	0.0064
84.162	C_6H_{12}	cyclohexane	AWAS	0.0022	0.0019	0.0026	0.008±0.014[3]	0.0064	0.0097
85.062	$C_3H_3NO_2$	methyl cyanoformate*	PTRMS	0.0011±0.0007	0.00068±0.0011	0.0016±0.00082		0.0018±0.029	0.0051±0.0025
85.106	C_4H_7NO	C_4H_5N water cluster*	PTRMS	0.00071±0.00037	0.00067±0.00015	0.00076±0.00072		0.0017±0.0034	0.0024±0.0021
86.09	$C_4H_6O_2$	methacrylic acid	CIMS	0.1±0.024	0.11±0.012	0.097±0.047		0.33±0.034	0.41±0.051
86.09	$C_4H_6O_2$	butanedione/isomers *	PTRMS	0.13±0.016	0.13±0.016	0.13±0.028	0.34[1] 0.42±0.17[2] 0.53±0.21[3]	0.33±0.034	0.41±0.051
86.134	$C_5H_{10}O$	pentanone*	PTRMS	0.046±0.0038	0.053±0.0058	0.038±0.0048		0.0095±0.0061	0.008±0.005
86.178	C_6H_{14}	n-hexane	AWAS	0.049	0.053	0.044	0.054±0.035[1] 0.04±0.036[3]	0.17	0.16
86.178	C_6H_{14}	2,3 dimethylbenzene	AWAS	0.0031	0.004	0.0022		0.014	0.0066
86.178	C_6H_{14}	2,3-methylpentane	AWAS	0.01	0.0089	0.011	0.01±0.0065[3]	0.032	0.039
88.062	$C_3H_4O_3$	pyruvic acid	CIMS	0.72±0.34	0.56±0.13	0.89±0.66	0.012±0.0047[2] 0.019±0.008[3]	0.022±0.012	-0.0025±0.02

https://doi.org/10.5194/acp-2022-245
Preprint. Discussion started: 14 April 2022

Atmospheric Chemistry and Physics Discussions

88.106	$C_4H_8O_2$	C4 saturated carboxylic acids	CIMS	0.082±0.023	0.12±0.044	0.047±0.012		0.13±0.053	0.16±0.052
88.106	$C_4H_8O_2$	methyl propanoate*	PTRMS	0.07±0.078	0.075±0.01	0.065±0.012	0.073±0.023[2] 0.081±0.036[3]	0.19±0.019	0.2±0.014
88.168	C_4H_8OS	oxathiane*	PTRMS	0.0031±0.0018	0.0023±0.0017	0.004±0.0032		0.0058±0.0041	0.012±0.0088
90.122	$C_4H_{10}O_2$	MEK water cluster/butane diol*	PTRMS	0.0017±0.00051	0.0017±0.00032	0.0016±0.00097		0.0041±0.0084	0.005±0.0029
90.125	C_7H_6	*	PTRMS	0.0069±0.0012	0.0064±0.0018	0.0074±0.0017		0.016±0.0044	0.022±0.0032
90.184	$C_4H_{10}S$	diethyl sulfide, butanethiol	PTRMS	0.077±0.0084	0.083±0.0077	0.071±0.015		0.2±0.028	0.21±0.04
91.113	C_6H_5N	ethylnylpyrrole*	PTRMS	0.0015±0.00069	0.0018±0.0013	0.0011±0.00031	0.0018±0.00088[2] 0.0091±0.0026[3]	0.0044±0.0031	0.0033±0.00054
92.141	C_7H_8	toluene	PTRMS	0.26±0.077	0.26±0.014	0.26±0.15	0.35±0.11[1] 0.25±0.13[2] 0.42±0.16[3]	0.63±0.01	0.71±0.38
93.082	$C_2H_7NO_3$	*	PTRMS	0.0025±0.00046	0.0025±0.00028	0.0025±0.00088		0.006±0.0009	0.007±0.0019
93.085	C_5H_3NO	furancarbonitrile*	PTRMS	0.02±0.0016	0.022±0.0018	0.018±0.0026	0.0026±0.001[2] 0.0088±0.0037[3]	0.053±0.0033	0.053±0.0031
93.129	C_6H_7N	methyl pyridine*	PTRMS	0.0017±0.00059	0.0017±0.0011	0.0017±0.00049	0.014±0.0073[2] 0.035±0.012[3]	0.004±0.0025	0.0047±0.0011
94.113	C_6H_6O	phenol*	PTRMS	0.12±0.018	0.12±0.014	0.12±0.033	0.57±0.36[2] 0.33±0.13[3]	0.28±0.031	0.35±0.053
94.13	$C_2H_6O_2S$	dimethyl sulfone*	PTRMS	0.0042±0.00079	0.0048±0.0013	0.0035±0.00086		0.055±0.02	0.015±0.0021
94.157	C_7H_{10}	cycloheptadiene*	PTRMS	0.021±0.0034	0.023±0.0028	0.02±0.0061		0.053±0.0046	0.056±0.012
94.19	$C_2H_6S_2$	dimethyl disulfide*	PTRMS	0.0041±0.00097	0.0044±0.0014	0.0039±0.0013	0.0024±0.0009[2]	0.01±0.003	0.011±0.026
95.077	$C_5H_3O_2$	*	PTRMS	0.0041±0.00031	0.0043±0.00039	0.0038±0.00048		0.0099±0.013	0.011±0.016
95.101	C_5H_5NO	pyridinol*	PTRMS	0.0022±0.0006	0.0021±0.00069	0.0023±0.00097	0.0099±0.0054[2]	0.0048±0.017	0.0063±0.0023
95.145	C_6H_9N	C2 pyrrole*	PTRMS	0.0024±0.00023	0.0027±0.00034	0.0021±0.00031		0.0063±0.0066	0.006±0.0046
96.085	$C_5H_4O_2$	furfural*	PTRMS	0.65±0.08	0.67±0.044	0.64±0.15	0.61[1] 0.54±0.17[2] 0.53±0.21[3]	1.5±0.045	1.8±0.23
96.129	C_6H_8O	C2-furan*	PTRMS	0.087±0.011	0.086±0.0063	0.087±0.022		0.2±0.018	0.24±0.033
96.173	C_7H_{12}	cycloheptene*	PTRMS	0.022±0.0029	0.033±0.0047	0.011±0.0034		0.076±0.01	0.031±0.081
97.073	$C_4H_3NO_2$	*	PTRMS	0.004±0.0022	0.0044±0.0035	0.0036±0.0028		0.0098±0.0076	0.0096±0.0072
97.117	C_5H_7NO	*	PTRMS	0.002±0.00039	0.0023±0.0004	0.0017±0.00066		0.0054±0.011	0.0045±0.0014
97.161	$C_6H_{11}N$	hexanenitrile*	PTRMS	0.004±0.00043	0.0041±0.00018	0.004±0.00083	0.0088±0.0047[3]	0.0093±0.0029	0.011±0.014
98.057	$C_4H_2O_3$	maleic anhydride*	PTRMS	0.07±0.013	0.072±0.011	0.068±0.023	0.14±0.072[3]	0.16±0.018	0.18±0.044

https://doi.org/10.5194/acp-2022-245
Preprint. Discussion started: 14 April 2022

Atmospheric Chemistry and Physics Discussions

98.101	$C_5H_6O_2$	furan methanol/isomers*	PTRMS	0.058±0.01	0.061±0.0059	0.054±0.019	0.38±0.15[2] 0.09±0.043[3]	0.14±0.009	0.15±0.038
98.145	$C_6H_{10}O$	methyl cyclopentanone/isomers*	PTRMS	0.015±0.0014	0.017±0.0013	0.013±0.0025	0.022±0.0086[2] 0.034±0.015[3]	0.038±0.0022	0.035±0.0039
98.163	C_5H_6S	methyl thiophene	PTRMS	0.0059±0.0045	0.0069±0.006	0.0048±0.0068	0.021±0.012[2]	0.017±0.015	0.013±0.017
98.189	C_7H_{14}	heptene*	PTRMS	0.0039±0.0011	0.0059±0.0019	0.0019±0.00089		0.013±0.0038	0.0054±0.002
100.117	$C_5H_8O_2$	unsaturated C5 carboxylic acids	CIMS	0.072±0.017	0.1±0.015	0.045±0.029		0.22±0.026	0.13±0.085
100.117	$C_5H_8O_2$	methyl methacrylate/isomers*	PTRMS	0.036±0.009	0.035±0.0077	0.037±0.016	0.14±0.053[2] 0.11±0.045[3]	0.078±0.016	0.098±0.036
100.161	$C_6H_{12}O$	hexanal/hexanones*	PTRMS	0.0065±0.00079	0.0074±0.001	0.0057±0.0012	0.0046±0.0029[2] 0.013±0.0056[3]	0.016±0.002	0.015±0.002
100.205	C_7H_{16}	2,2,3-trimethylbutane	AWAS	0.00062	0.00067	0.00057		0.0018	0.0015
100.205	C_7H_{16}	3,3-dimethylpentane	AWAS	0.035	0.054	0.016		0.15	0.052
100.205	C_7H_{16}	3-methylhexane	AWAS	0.0075	0.0090	0.0060	0.016±0.018[3]	0.027	0.017
102.089	$C_4H_6O_3$	C4 oxo-carboxylic acids	CIMS	0.74±0.22	0.57±0.1	0.92±0.43		1.2±0.26	2.4±0.89
102.089	$C_4H_6O_3$	acetic anhydride*	PTRMS	0.0075±0.0015	0.0078±0.00036	0.0072±0.003	0.089±0.034[2] 0.044±0.02[3]	0.017±0.00064	0.019±0.068
102.133	$C_5H_{10}O_2$	C5 saturated carboxylic acids	CIMS	0.012±0.0052	0.018±0.004	0.0055±0.0096		0.039±0.01	0.016±0.027
102.133	$C_5H_{10}O_2$	valeric acid*	PTRMS	0.024±0.0044	0.027±0.0036	0.02±0.0081		0.059±0.0067	0.052±0.016
102.177	$C_6H_{14}O$	hexanol*	PTRMS	0.002±0.00032	0.0022±0.00054	0.0017±0.00033		0.0047±0.0098	0.0045±0.00075
103.121	$C_4H_9NO_2$	*	PTRMS	0.0069±0.0011	0.0074±0.00091	0.0064±0.0019		0.016±0.0014	0.016±0.039
103.124	C_7H_5N	benzonitrile*	PTRMS	0.06±0.0044	0.065±0.0021	0.054±0.0086	0.021±0.0045[2] 0.055±0.022[3]	0.14±0.0025	0.14±0.0088
103.165	$C_5H_{13}NO$	*	PTRMS	0.0011±0.00028	0.0013±0.00013	0.00095±0.00054		0.0028±0.0026	0.0025±0.0014
104.108	C_7H_4O	*	PTRMS	0.0019±0.00043	0.0021±0.00024	0.0017±0.00083		0.0045±0.005	0.0043±0.0018
104.149	$C_5H_{12}O_2$	pentanediol*	PTRMS	0.0029±0.00082	0.0033±0.0013	0.0024±0.001		0.0069±0.025	0.006±0.022
104.152	C_8H_8	styrene*	PTRMS	0.039±0.0027	0.056±0.0014	0.022±0.0053	0.088±0.056[2] 0.018±0.012[3]	0.12±0.0024	0.058±0.089
106.121	$C_4H_{10}O_3$	diethylene glycol*	PTRMS	0.0048±0.0019	0.006±0.0022	0.0036±0.003		0.012±0.0042	0.0088±0.0067
106.124	C_7H_6O	benzaldehyde*	PTRMS	0.036±0.0035	0.042±0.0012	0.03±0.0069	0.095±0.053[2] 0.084±0.026[3]	0.087±0.0029	0.077±0.088
106.168	C_8H_{10}	C8 aromatics	PTRMS	0.075±0.0069	0.082±0.0065	0.068±0.012	0.12±0.052[2] 0.21±0.08[3]	0.17±0.013	0.17±0.0099

https://doi.org/10.5194/acp-2022-245
Preprint. Discussion started: 14 April 2022

Atmospheric Chemistry and Physics Discussions

107.112	C_6H_5NO	pyridine aldehyde*	PTRMS	0.0012±0.00024	0.00094±0.00032	0.0015±0.00035		0.0019±0.00067	0.0038±0.00063
107.156	C_7H_9N	dimethyl pryidine/heptyl nitriles*	PTRMS	0.0016±0.00048	0.0015±0.00042	0.0018±0.00087	0.005±0.0033[2]	0.0031±0.0075	0.0043±0.0019
108.096	$C_6H_4O_2$	benzoquinone/quinone*	PTRMS	0.025±0.004	0.024±0.0027	0.025±0.0076	0.084±0.024[2] 0.077±0.02[3]	0.049±0.007	0.062±0.013
108.14	C_7H_8O	methyl phenol/anisol/cresol*	PTRMS	0.04±0.0055	0.04±0.0063	0.04±0.009	0.41±0.17[2] 0.23±0.11[3]	0.083±0.015	0.099±0.011
108.184	C_8H_{12}	cyclooctadiene*	PTRMS	0.015±0.0018	0.017±0.00037	0.013±0.0036		0.034±0.0014	0.032±0.052
109.104	$C_6H_5O_2$	*	PTRMS	0.0055±0.00065	0.0055±0.00067	0.0055±0.0011		0.011±0.0015	0.014±0.028
109.128	C_6H_7NO	*	PTRMS	0.002±0.0011	0.0017±0.00039	0.0024±0.0021		0.0035±0.0075	0.0057±0.005
110.112	$C_6H_6O_2$	benzenediol/methyl furfural*	PTRMS	0.11±0.015	0.11±0.005	0.11±0.03	0.68±0.29[2] 0.25±0.12[3]	0.21±0.0056	0.27±0.044
110.156	$C_7H_{10}O$	norcamphor/C3 furan*	PTRMS	0.032±0.004	0.03±0.0029	0.034±0.0076	0.079±0.026[2] 0.046±0.024[3]	0.059±0.0039	0.083±0.01
110.2	C_8H_{14}	cyclooctene*	PTRMS	0.0088±0.0019	0.012±0.0027	0.0053±0.0026		0.024±0.0047	0.014±0.059
111.1	$C_5H_5NO_2$	dihydroxy piridine/methyl maleimide*	PTRMS	0.0026±0.00081	0.0031±0.0004	0.0022±0.0016	0.0066±0.0023[2] 0.024±0.0084[3]	0.0061±0.0069	0.0051±0.0036
111.144	C_6H_9NO	*	PTRMS	0.0018±0.00032	0.0028±0.00056	0.00091±0.003		0.0054±0.0092	0.0023±0.00057
112.084	$C_5H_4O_3$	furoic acid/hydroxy furfural*	PTRMS	0.041±0.0081	0.044±0.0041	0.038±0.016	0.11±0.043[2] 0.12±0.031[3]	0.087±0.0049	0.089±0.029
112.128	$C_6H_8O_2$	cyclohexanedione*	PTRMS	0.014±0.0019	0.014±0.0034	0.014±0.0017		0.028±0.0081	0.033±0.041
112.172	$C_7H_{12}O$	ethylcyclohe ptanone*	PTRMS	0.0069±0.0017	0.0067±0.001	0.007±0.0032	0.012±0.0056[2] 0.014±0.007[3]	0.013±0.0014	0.016±0.061
112.19	C_6H_8S	dimethylthiophene	PTRMS	0.023±0.0098	0.028±0.016	0.018±0.012		0.055±0.029	0.042±0.025
112.216	C_8H_{16}	octene*	PTRMS	0.0017±0.00079	0.0021±0.0014	0.0013±0.00082		0.0042±0.025	0.0027±0.0021
114.144	$C_6H_{10}O_2$	sum of cyclic saturated and n-unsaturated C5 carboxylic acids	CIMS	0.0018±0.00026	0.0029±0.00038	0.00065±0.0035		0.0025±0.0075	0.0014±0.00085
114.144	$C_6H_{10}O_2$	caprolactone/c6 esters/ c6 diketone isomers*	PTRMS	0.0068±0.0011	0.0082±0.00098	0.0053±0.0021	0.034±0.014[2] 0.039±0.017[3]	0.016±0.0014	0.013±0.043
114.188	$C_7H_{14}O$	heptanone/heptanal/isomers*	PTRMS	0.005±0.00078	0.006±0.0012	0.0039±0.001	0.0091±0.0045[2] 0.0072±0.0025[3]	0.012±0.0019	0.009±0.013
114.232	C_8H_{18}	2,2-dimethylhexane	AWAS	0.0029	0.0036	0.0022		0.0095	0.0056

https://doi.org/10.5194/acp-2022-245
Preprint. Discussion started: 14 April 2022

Atmospheric Chemistry and Physics Discussions

114.232	C_8H_{18}	4-methylheptane	AWAS	0.015	0.015	0.015		0.037	0.041
116.116	$C_5H_8O_3$	C5 oxo-carboxylic acids	CIMS	1.3±0.35	1.1±0.15	1.5±0.68		2±0.34	3.4±1.2
116.143	C_8H_6N	*	PTRMS	0.0028±0.00063	0.0035±0.0011	0.0021±0.00068		0.0065±0.0018	0.0049±0.0011
116.16	$C_6H_{12}O_2$	C6 saturated carboxylic acids	CIMS	0.0001±0.00041	0.00013±0.00075	7.5E-5±0.00032		0.00019±0.0014	0.00024±0.00079
116.16	$C_6H_{12}O_2$	butyl acetate/c6 esters *	PTRMS	0.0073±0.0015	0.0094±0.0013	0.0052±0.0028	0.012±0.0081[2] 0.011±0.0062[3]	0.018±0.0018	0.012±0.0056
116.204	$C_7H_{16}O$	heptanol*	PTRMS	0.0018±0.00043	0.0016±0.00037	0.0019±0.00078		0.0031±0.0074	0.0043±0.0015
116.222	$C_6H_{12}S$	cyclohexanethiol*	PTRMS	0.0032±0.0012	0.004±0.0012	0.0025±0.0021		0.0075±0.002	0.0056±0.0042
118.088	$C_4H_6O_4$	succinic acid*	PTRMS	0.0017±0.00029	0.0026±0.00049	0.00081±0.0031		0.0048±0.0076	0.0018±0.00055
118.135	C_8H_6O	benzofuran*	PTRMS	0.017±0.0017	0.018±0.00066	0.017±0.0034	0.037±0.02[2] 0.041±0.015[3]	0.034±0.0027	0.038±0.003
118.179	C_9H_{10}	methylstyrenes/propenyl benzenes*	PTRMS	0.018±0.0014	0.024±0.0012	0.011±0.0026	0.05±0.03[2] 0.037±0.019[3]	0.046±0.00075	0.025±0.0047
119.123	C_7H_5NO	*	PTRMS	0.00094±0.00021	0.0011±0.00013	0.0008±0.00041		0.002±0.00016	0.0018±0.00077
119.167	C_8H_9N	*	PTRMS	0.0018±0.00018	0.002±8.4E-5	0.0016±0.00036		0.0037±0.0028	0.0035±0.00042
120.151	C_8H_8O	methylbenzaldehyde/tolualdehyde*	PTRMS	0.025±0.0037	0.024±0.0011	0.026±0.0073	0.13±0.08[2] 0.082±0.03[3]	0.044±0.0017	0.058±0.0097
120.195	C_9H_{12}	trimethylbenzene/C9 aromatics*	PTRMS	0.052±0.0061	0.075±0.011	0.029±0.0056	0.051±0.02[2] 0.069±0.031[3]	0.14±0.015	0.064±0.0079
120.195	C_9H_{12}	Isopropylbenzene	AWAS	0.013	0.011	0.016	0.013±0.025[3]	0.025	0.040
120.195	C_9H_{12}	n-propylbenzene	AWAS	0.27	0.30	0.24	0.0064±0.0039[3]	0.69	0.59
120.195	C_9H_{12}	1,3,5-trimethylbenzene	AWAS	0.062	0.081	0.043	0.0036±0.0027[3]	0.19	0.11
120.195	C_9H_{12}	1-methyl-2-ethylbenzene	AWAS	0.81	0.83	0.78		1.9	2.0
121.139	C_7H_7NO	*	PTRMS	0.00095±0.00033	0.00091±0.00023	0.001±0.00061		0.0016±0.0038	0.0022±0.0012
122.123	$C_7H_6O_2$	benzoic acid/hydroxybenzaldehyde*	PTRMS	0.02±0.0038	0.021±0.00058	0.019±0.0075	0.079±0.035[2] 0.065±0.023[3]	0.037±0.0016	0.04±0.013
122.167	$C_8H_{10}O$	xylenol/C2phenol/methylanisole*	PTRMS	0.015±0.0018	0.016±0.00096	0.013±0.0035	0.11±0.037[2] 0.1±0.057[3]	0.029±0.0027	0.029±0.0051
122.211	C_9H_{14}	cyclohexylalleene*	PTRMS	0.0076±0.001	0.0083±0.0017	0.0068±0.0012		0.015±0.0028	0.015±0.0091

https://doi.org/10.5194/acp-2022-245
Preprint. Discussion started: 14 April 2022

Atmospheric Chemistry and Physics Discussions

124.095	$C_6H_4O_3$	hydroxy benzoquinone*	PTRMS	0.0032±0.0012	0.0029±0.00083	0.0035±0.0022	0.073±0.018[2] 0.045±0.026[3]	0.0051±0.0015	0.0075±0.0042
124.139	$C_7H_8O_2$	guaiacol*	PTRMS	0.052±0.007	0.051±0.0086	0.053±0.011	0.37±0.12[2] 0.27±0.17[3]	0.091±0.019	0.12±0.014
124.183	$C_8H_{12}O$	acetylcyclohexene*	PTRMS	0.0078±0.0011	0.0087±0.0015	0.0068±0.0016		0.015±0.0021	0.015±0.017
124.227	C_9H_{16}	cyclononene*	PTRMS	0.0022±0.00033	0.0022±0.00048	0.0022±0.00046		0.0039±0.0072	0.0048±0.00061
126.111	$C_6H_6O_3$	hydroxymethylfurfural*	PTRMS	0.0096±0.002	0.0094±0.0031	0.0098±0.0027	0.27±0.1[2] 0.064±0.026[3]	0.016±0.0054	0.021±0.035
126.155	$C_7H_{10}O_2$	unsaturated C6 cyclic carboxylic acid	CIMS	0.012±0.0053	0.015±0.0073	0.0087±0.0076		0.026±0.012	0.019±0.016
126.155	$C_7H_{10}O_2$	cyclohexene carboxylic acid *	PTRMS	0.0064±0.0019	0.008±0.0035	0.0048±0.0016		0.014±0.0056	0.01±0.0025
126.199	$C_8H_{14}O$	octenone*	PTRMS	0.0032±0.00064	0.0037±0.00064	0.0027±0.0011		0.0064±0.012	0.0057±0.0018
126.217	$C_7H_{10}S$	trimethylthiophene*	PTRMS	0.011±0.00091	0.016±0.0013	0.0054±0.0013		0.028±0.0027	0.012±0.019
126.243	C_9H_{18}	cis,trans,trans-1,2,4-trimethylcyclohexane	AWAS	0.0019	0.0022	0.0016		0.0046	0.0033
126.243	C_9H_{18}	1-nonene	AWAS	0.00010	4.7E-05	0.00016		- 0.00015	0.00039
128.127	$C_6H_8O_3$	di hydroxymethyl furan*	PTRMS	0.0044±0.0009	0.0059±0.0014	0.0029±0.0012		0.01±0.0025	0.0063±0.0026
128.171	$C_7H_{12}O_2$	C6 unsaturated carboxylic acids	CIMS	0.0091±0.0032	0.011±0.0031	0.0077±0.0055		0.018±0.0048	0.016±0.011
128.171	$C_7H_{12}O_2$	cyclohexanoic acid*	PTRMS	0.0068±0.0017	0.0085±0.0029	0.005±0.0018		0.015±0.0044	0.01±0.0028
128.174	$C_{10}H_8$	naphthalene*	PTRMS	0.017±0.0035	0.018±0.0037	0.015±0.0059	0.078±0.056[2]	0.031±0.0056	0.031±0.096
128.215	$C_8H_{16}O$	octanone*	PTRMS	0.0034±0.00044	0.0039±0.0006	0.0028±0.00065		0.0068±0.0078	0.006±0.012
128.259	C_9H_{20}	3,3-diethylpentane	AWAS	0.0075	0.0055	0.0094		0.011	0.022
130.187	$C_7H_{14}O_2$	C7 saturated carboxylic acids	CIMS	0.022±0.0069	0.026±0.013	0.018±0.0036		0.043±0.021	0.037±0.0097
130.187	$C_7H_{14}O_2$	amyl acetate*	PTRMS	0.0031±0.00078	0.0034±0.0013	0.0028±0.00088		0.0056±0.002	0.0058±0.0014
132.159	$C_6H_{12}O_3$	C6 hydroxy-carboxylic acids	CIMS	0.0016±0.00038	0.0027±0.00061	0.00053±0.00045		0.0045±0.0088	0.0012±0.001
132.162	C_9H_8O	methylbenzofurans*	PTRMS	0.01±0.016	0.01±0.001	0.011±0.003	0.055±0.03[2] 0.046±0.021[3]	0.017±0.0014	0.021±0.037
132.206	$C_{10}H_{12}$	ethylstyrene/ methylpropenyl benzene*	PTRMS	0.0083±0.0012	0.0083±0.0016	0.0083±0.0017	0.041±0.019[2] 0.04±0.026[3]	0.014±0.0031	0.017±0.014
134.134	$C_8H_6O_2$	phthalic acid*	PTRMS	0.0039±0.0011	0.0044±0.0016	0.0033±0.0014		0.0071±0.023	0.0065±0.0024

https://doi.org/10.5194/acp-2022-245
Preprint. Discussion started: 14 April 2022

Atmospheric Chemistry and Physics Discussions

134.178	$C_9H_{10}O$	methylacetophenone*	PTRMS	0.0059±0.00094	0.0062±0.00043	0.0056±0.0018	0.053±0.031[2] 0.045±0.019[3]	0.01±0.00064	0.011±0.0026
134.222	$C_{10}H_{14}$	C10 aromatics*	PTRMS	0.024±0.0019	0.035±0.002	0.013±0.0033	0.043±0.022[2] 0.04±0.021[3]	0.058±0.0022	0.026±0.0052
134.222	$C_{10}H_{14}$	1,2-diethylbenzene	AWAS	1.3	1.6	1.1		3.3	2.6
134.222	$C_{10}H_{14}$	1,2-dimethyl-4-ethylbenzene	AWAS	0.063	0.085	0.042		0.19	0.094
134.222	$C_{10}H_{14}$	1,4-dimethyl-2-ethylbenzene	AWAS	0.11	0.089	0.13		0.15	0.31
136.15	$C_8H_8O_2$	methyl benzoic acid*	PTRMS	0.013±0.0013	0.014±0.0014	0.012±0.0022	0.081±0.03[2] 0.066±0.029[3]	0.022±0.0014	0.023±0.0028
136.238	$C_{10}H_{16}$	monoterpenes	PTRMS	0.39±0.034	0.49±0.0094	0.29±0.068	1.53[1] 0.87±0.72[2] 0.21±0.15[3]	0.8±0.032	0.57±0.13
138.122	$C_7H_6O_3$	hydroxybenzoic acid*	PTRMS	0.0026±0.00061	0.0039±0.0012	0.0014±0.00028		0.0061±0.017	0.0028±0.00035
138.166	$C_8H_{10}O_2$	creosol/methyl guiacol*	PTRMS	0.0073±0.0013	0.0077±0.0014	0.0069±0.0022	0.26±0.077[2] 0.14±0.11[3]	0.012±0.0019	0.013±0.0033
138.21	$C_9H_{14}O$	isophorone*	PTRMS	0.0092±0.0016	0.0086±0.0015	0.0098±0.0028		0.014±0.0027	0.019±0.0039
142.286	$C_{10}H_{22}$	3,3-dimethyloctane	AWAS	0.078	0.0020	0.15		-0.071	0.37
146.189	$C_{10}H_{10}O$	dimethylbenzofuran/ethyl benzofuran*	PTRMS	0.0048±0.00051	0.0052±0.00085	0.0045±0.00058	0.043±0.018[2] 0.051±0.028[3]	0.0078±0.011	0.0083±0.00035
146.233	$C_{11}H_{14}$	*	PTRMS	0.0035±0.0007	0.0037±0.00059	0.0034±0.0013		0.0057±0.011	0.0061±0.0019
148.117	$C_8H_4O_3$	benzofurandione*	PTRMS	0.0047±0.0012	0.0048±0.0013	0.0047±0.002		0.0071±0.017	0.0082±0.003
148.161	$C_9H_8O_2$	cinnamic acid*	PTRMS	0.0024±0.00062	0.0026±4.2E-5	0.0021±0.0012		0.0039±0.0015	0.0037±0.0019
148.205	$C_{10}H_{12}O$	benzylacetone/estragole*	PTRMS	0.0023±0.00054	0.0022±0.00088	0.0024±0.00063	0.027±0.012[2] 0.025±0.015[3]	0.0033±0.014	0.0044±0.00074
148.249	$C_{11}H_{16}$	C11 aromatics/pentamethylbenzene*	PTRMS	0.0041±0.00069	0.0043±0.00057	0.0038±0.0013	0.014±0.0078[2] 0.014±0.0074[3]	0.0064±0.0082	0.0069±0.0016
150.177	$C_9H_{10}O_2$	ethyl benzoate/vinyl guaiacol*	PTRMS	0.0028±0.00045	0.0029±0.00052	0.0028±0.0073	0.14±0.076[2] 0.036±0.025[3]	0.0043±0.0079	0.0049±0.0009
150.221	$C_{10}H_{14}O$	carvone*	PTRMS	0.0021±0.00049	0.0027±0.0009	0.0015±0.0039		0.0039±0.012	0.0027±0.00048
152.149	$C_8H_8O_3$	methoxybenzoic acid*	PTRMS	0.0075±0.0019	0.0085±0.0025	0.0065±0.0029		0.012±0.0032	0.011±0.0041
152.193	$C_9H_{12}O_2$	ethylguaiacol*	PTRMS	0.0027±0.001	0.0031±0.0018	0.0022±0.00098		0.0044±0.024	0.0039±0.0014
152.196	$C_{12}H_8$	acenaphthylene*	PTRMS	0.0032±0.0011	0.0041±0.0021	0.0022±0.0089	0.01±0.0066[2]	0.0059±0.028	0.0038±0.0012
152.237	$C_{10}H_{16}O$	camphor/isomers*	PTRMS	0.011±0.0015	0.013±0.0022	0.0087±0.002	0.027±0.017[2] 0.025±0.014[3]	0.02±0.0033	0.015±0.0026
154.165	$C_8H_{10}O_3$	syringol*	PTRMS	0.0022±0.00045	0.0026±0.00056	0.0017±0.0007	0.022±0.0078[2] 0.017±0.0067[3]	0.0037±0.0065	0.0029±0.001

https://doi.org/10.5194/acp-2022-245
Preprint. Discussion started: 14 April 2022

Atmospheric Chemistry and Physics Discussions

154.209	$C_9H_{14}O_2$	norbornaneacetic acid*	PTRMS	0.0022±0.00083	0.0023±0.0011	0.0022±0.0012		0.0033±0.017	0.0038±0.0018
154.212	$C_{12}H_{10}$	acenaphthene*	PTRMS	0.0029±0.00052	0.0033±0.00033	0.0025±0.00099		0.0046±0.003	0.0042±0.0014
154.253	$C_{10}H_{18}O$	terpine-4-ol/cineole/isomers*	PTRMS	0.0018±0.00065	0.0019±0.00084	0.0017±0.00098	0.0056±0.0021[2] 0.0027±0.0017[3]	0.0029±0.014	0.0028±0.0015
204.357	$C_{15}H_{24}$	sesquiterpenes*	PTRMS	0.0021±0.00032	0.0024±0.00045	0.0017±0.00045	0.15±0.07[2] 0.029±0.028[3]	0.0026±0.0038	0.0022±0.00047
239±61	C_{11} to C_{25}	I/SVOCs – C_xH_y	cartridge	1.6±0.04					
255±61	C_{11} to C_{25}	I/SVOCs – $C_xH_yO_1$	cartridge	0.9±0.09					
271±61	C_{11} to C_{25}	I/SVOCs – $C_xH_yS_1$	cartridge	0.1±0.003					

1426